

Buoyancy-driven fluid and energy flow in protruded heater enclosure

Nirmalendu Biswas · Pallab Sinha Mahapatra ·
Nirmal Kumar Manna

Received: 2 August 2015 / Accepted: 7 January 2016 / Published online: 28 January 2016
© Springer Science+Business Media Dordrecht 2016

Abstract Flow structures and thermal aspects of buoyancy-driven flow occurring in the presence of protruded heater inside a square enclosure are investigated under different thermal boundary conditions of the enclosure for two common fluids (of Prandtl numbers $Pr = 0.71$ and 6.9) at various Rayleigh numbers ($Ra = 10^3$ – 10^6) numerically. The study is conducted considering a single heater as well as a set of two identical heaters located symmetrically on the bottom wall of the enclosure. Results reveals that the heat transfer, energy flow and fluid flow are markedly dependent on the heater aspect ratio, Ra , Pr and thermal boundary condition. Although with the single heater symmetric trends of fluid and heat flow are observed, the strong asymmetric flow features are found in case of the double heaters for $Pr = 6.9$ at higher Ra . Some interesting energy and fluid flow patterns are evolved depending upon the values of heater aspect ratio, interspatial heater distance and enclosure's boundary condition. The visualization of

mass and energy transports are properly appreciated using streamfunction and heatfunction. Total fluid flow inside the enclosure is analyzed by applying a novel approach based on streamfunctions of thermally induced vortices, which is also used to formulate a new streamfunction based symmetry indicator. It is seen that, with the increase in heater height although the total flow decreases, a consistent trend of increasing heat transfer is observed. The nature of steady-state solutions for the cavity is also analyzed by gradually increasing and decreasing Ra . Symmetry breaking bifurcation has been identified for $Pr = 6.9$. The bifurcation characteristics changes from supercritical to subcritical bifurcation depending upon thermal boundary conditions of the enclosure.

Keywords Protruded heater · Natural convection · Heatlines · Heat transfer · Supercritical bifurcation · Subcritical bifurcation · Vortical structure based symmetry indicator

N. Biswas · N. K. Manna (✉)
Department of Mechanical Engineering, Jadavpur
University, Kolkata 700 032, India
e-mail: nirmalendubiswas@yahoo.co.in

N. K. Manna
e-mail: nirmalkmannaju@gmail.com

P. S. Mahapatra
Department of Mechanical and Industrial Engineering,
UIC, Chicago, IL, USA
e-mail: pallabju@gmail.com

List of symbols

A	Heater aspect ratio
d	Distance between two heaters
D	Dimensionless interspatial distance
g	Acceleration due to gravity
h	Heater height
H	Dimensionless heater height
I_θ	Symmetry indicator based on θ
I_ψ	Symmetry indicator based on ψ
L	Length/height of the enclosure

Nu	Nusselt number
p	Pressure
P	Dimensionless pressure
Pr	Prandtl number
q_i	Dimensionless total heat inflow
q_o	Dimensionless total heat outflow
Ra	Rayleigh number
SSC	Side-side cold condition
STSC	Side-top-side cold condition
T	Temperature
u, v	Velocity components
U, V	Dimensionless velocity components
w	Heater width
X, Y	Dimensionless Cartesian coordinates

Greek symbols

α	Thermal diffusivity
β	Volumetric expansion coefficient
θ	Dimensionless temperature
ν	Kinematic viscosity
Π	Dimensionless heat function
ρ	Fluid density
τ	Dimensionless time
Ψ	Dimensionless streamfunction

Subscripts

$1H, 2H$	One heater, two heaters
$1HE$	Single heater enclosure
$2HE$	Double heater enclosure
a	Ambient
avg	Average
c, h	Cold wall, hot wall
max	Maximum
min	Minimum
tot	Total

1 Introduction

Apart from different natural manifestations, free or natural convection finds widespread applications in many industrial and engineering fields. For instance, natural convection is frequently used for cooling of electronic devices, where undesirable heat is generated as a by-product of normal operation. Natural convection is also very common in several other engineering and environmental applications. Solar

energy, pond, lake and reservoir, air conditioning and ventilation, nuclear reactor, energy storage, furnace, heat exchanger, materials processing like solidification and crystal growth, micro-fuel cell design, oceanic current, climate change, are just a few examples among many others. From long past to recent time, researchers have paid a considerable attention to study different types of natural convection problems. Extensive reviews exist on natural convection in locally heated enclosures [1–3]. Later, Narasimham [4] also furnished an extensive review on natural convection in connection with discrete heat sources in enclosures and pointed out the direction for further researches therein. Natural convection is extensively used for passive cooling of electronic devices [5, 6].

Aydin and Yang [7] numerically investigated natural convection of air in a square cavity with partial heating from below and symmetrical cooling through sidewalls considering isothermal heater and sidewalls. The same heater-enclosure-geometry but using iso-flux heater instead of isothermal heater, Sharif and Mohammad [8] investigated heat transfer process taking into account of inclination angle of a rectangular cavity. Calcagni et al. [9] conducted experimental as well as numerical study of natural convection in a square enclosure with discrete heat source at bottom and cold sidewalls. All these works have considered top wall (of the enclosure) as adiabatic, sidewalls as cold, and bottom wall (on which wall-mounted flushed heater is located) as adiabatic.

The study was also carried out using the protruded heater. Varol et al. [10] numerically analyzed natural convection using a protruding heater in a triangular enclosure, and found that the heater dimension affects the temperature distribution, flow field and heat transfer. Paroncini and Corvaro [11–13] and Nardini et al. [14] considered an isothermal protruded heater projected from the bottom wall of an enclosure, of which horizontal walls were insulated and vertical walls were cold. The effects of the position and height of this heater (width fixed) on heat transfer were analyzed for $Ra \leq 10^6$ using air ($Pr = 0.71$). AlAmiri et al. [15] also analyzed an isothermal protruded heater using air, but considered the width variation of the heater and suggested some heat transfer correlations using dimensionless groups. Bakkas et al. [16]

numerically explored the effects of inter-block spacing and block height on fluid flow and heat transfer characteristics, by periodically mounting rectangular hot blocks on the lower wall of a two-dimensional horizontal channel. Earlier, Baek et al. [17] carried out both experimental and numerical investigations of combined heat transfer of a heat source protruded from adiabatic vertical wall in a three dimensional enclosure. Dagtekin and Oztop [18] analyzed natural convection using two heated partitions in an enclosure, and found that, the position of partitions affects fluid flow more than heat transfer. None of these works used heatfunction and heatlines [19–22] to explain transport phenomenon of heat (or energy) flow in enclosures or channels.

Literature review shows that, though the study of natural convection using the flush-mounted heater (heating element lying along enclosure wall) was undertaken by many researchers, the study of natural convection using the protruded heater is addressed relatively less. Enclosure's thermal boundary condition always influence the heat transfer process. To explore the same an experimental and numerical study was conducted on a single protruded heater of constant perimeter considering sidewalls and top wall cold condition and is recently reported by Biswas et al. [23]. Present work is an extension of [23]. In the present work, the effect of change in thermal boundary condition of enclosure's walls is investigated systematically. When the protruded heater is located on the bottom, cooling through the sidewalls or cooling through both the sidewalls and top wall could be representative configuration for many applications such as electronic cooling. So both of these thermal conditions are applied in this work. Furthermore, the consideration of double protruded heaters at bottom is included on the purview higher heating load with restricted overall size. Both single and double protruded heaters are taken at different heights or aspect ratios. For double heaters, the effects of interspatial distance between two heaters are also taken into account. Two common working fluids, air and water, are utilized in this work. Consideration of water as working fluid is important for submerged cooling, which is relevant on the context of ever-increasing demand on effective heat removal from electronic components. In this respect, Alfieri et al. [24] reported a fundamental hydrothermal investigation of the integrated water cooled three-dimensional chip stacks,

with high volumetric heat generation. Kota et al. [25–27] also presented a novel conduction-natural convection based cooling solution for thermal management of 3D stacked electronics through immersion cooling.

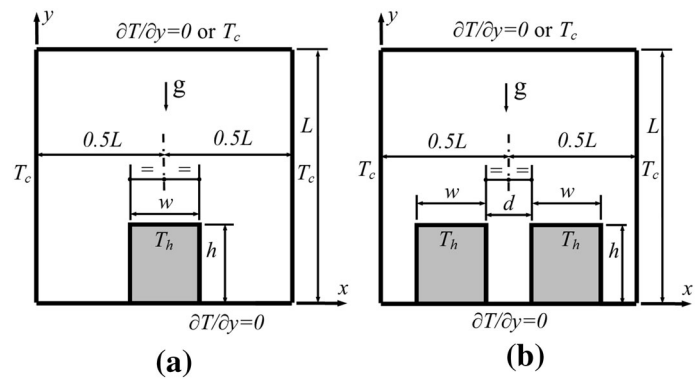
The major objective of this work is to analyze energy transport phenomena using heatlines [19–22] and to quantify overall heat transfer coefficient for the heater as well as the enclosure for all the cases as mentioned above. The consideration of Bejan's heatlines those are generated after solving heatfunction equations is very important for analysis and visualization of energy flow properly while the convection is sufficiently strong [19–22]. Moreover, a novel concept has been developed and implemented to estimate buoyancy-induced flow rate and degree of asymmetry by using the summation of maximal and minimal streamfunctions of individual vortices. A bifurcation analysis is also conducted to explore the nature of the evolved flow asymmetry in the cavity.

2 Problem definition, mathematical formulation and numerical procedure

The problem geometry considered consists of a square enclosure ($L \times L$) and rectangular heaters ($w \times h$) protruded from insulated bottom surface of the enclosure, as shown in Fig. 1. Two different configurations, one with single heater and other with two-identical heaters as shown in details in Fig. 1a, b, respectively, are considered in this study, where both the configurations are arranged symmetrically about the mid-vertical plane. The width (w) of the heater is taken fixed ($0.2L$), whereas its height (h) is varied from 0 (flush-mounted condition) to $0.5L$ maximum. The heater surface temperature is assumed to be maintained uniform of T_h . The thermal condition of the enclosure is governed by the surrounding ambient temperature (which acts as an isothermal heat sink at temperature T_c), so two different thermal conditions are implemented for the enclosure: one with cold sidewalls and top wall insulated, and other with all walls cold except the bottom wall. These conditions are applied to both the single and double heater enclosures, and for brevity, addressed by terms SSC (side-side cold) and STSC (side-top-side cold) in this work.

The analyses of fluid and energy flow, and heat transfer are carried out assuming unsteady

Fig. 1 Physical description of the enclosure with protruded heater(s). **a** Single heater enclosure, **b** double heater enclosure



incompressible Newtonian flow in a two-dimensional Cartesian geometry within the validity of Boussinesq approximation [28]. Furthermore, the viscous dissipation in energy equation is neglected following similar earlier works [10, 15, 21, 29]. Resulting dimensionless governing equations for mass, momentum and energy balances are formulated as

$$\frac{\partial U}{\partial X} + \frac{\partial V}{\partial Y} = 0 \quad (1)$$

$$\frac{\partial U}{\partial \tau} + U \frac{\partial U}{\partial X} + V \frac{\partial U}{\partial Y} = -\frac{\partial P}{\partial X} + \text{Pr} \left(\frac{\partial^2 U}{\partial X^2} + \frac{\partial^2 U}{\partial Y^2} \right) \quad (2)$$

$$\frac{\partial V}{\partial \tau} + U \frac{\partial V}{\partial X} + V \frac{\partial V}{\partial Y} = -\frac{\partial P}{\partial Y} + \text{Pr} \left(\frac{\partial^2 V}{\partial X^2} + \frac{\partial^2 V}{\partial Y^2} \right) + \text{Ra} \text{Pr} \theta \quad (3)$$

$$\frac{\partial \theta}{\partial \tau} + U \frac{\partial \theta}{\partial X} + V \frac{\partial \theta}{\partial Y} = \left(\frac{\partial^2 \theta}{\partial X^2} + \frac{\partial^2 \theta}{\partial Y^2} \right) \quad (4)$$

where, Prandtl number (Pr) and Rayleigh number (Ra) are defined as

$$\text{Pr} = \frac{\nu}{\alpha} \text{ and } \text{Ra} = \frac{g\beta(T_h - T_c)L^3}{\nu^2} \text{Pr}$$

respectively, and the definitions of dimensionless variables are described by

$$(X, Y) = \frac{(x, y)}{L}; (U, V) = \frac{(u, v)}{\alpha/L};$$

$$P = \frac{(p + \rho gy) - p_a}{\rho \alpha^2 / L^2}, \theta = \frac{T - T_c}{T_h - T_c}, \text{ and}$$

$$\tau = \frac{t}{L^2 / \alpha}$$

where, u and v are the dimensional velocity components along the x and y axes, X and Y are dimensionless distances, t and τ are the dimensional and dimensionless time respectively. The dimensionless pressure P is defined considering both static pressure change (ρgy) and ambient pressure (p_a). The fluid properties utilized here are density ρ , kinematic viscosity ν , volumetric thermal expansion coefficient β , and thermal diffusivity α . Their values are taken as constant. However, the density variation for buoyancy force is addressed through β and local temperature different.

The thermal conditions of heater surfaces, and the cold and adiabatic walls of the enclosure are set by $\theta = 1, \theta = 0$ and $\partial\theta/\partial Y = 0$, respectively. Zero velocity ($U = V = 0$) is set at all enclosure walls and heater surfaces following no-slip and no-penetration conditions. With these boundary conditions, the governing equations are solved utilizing an in-house code based on Finite Volume Method (FVM), SIMPLE algorithm [30], Alternate Direction Implicit (ADI) sweep and Tri-Diagonal Matrix Algorithm (TDMA), iteratively. For the convergence of solutions, the maximum residual and continuity mass-defect are chosen less than 10^{-8} and 10^{-10} , respectively. The validation of the same code against the benchmark results has been presented earlier by Mahapatra et al. [29]. Further to it, one experimental validation, and another numerical validation against the results of AlAmiri et al. [15] have been conducted using a single protruded heater configuration, and found satisfactory. However, these validation results are reported recently in Biswas et al. [23] and can be found therein. The grid size for the present numerical simulation is chosen 100×100 , after performing a

grid independence study with four different grid sizes (40 × 40, 80 × 80, 100 × 100 and 150 × 150) following a non-uniform grid distribution.

In this work, heat transfer analyses for the single heater and two-heater enclosures are reported in nondimensional form in terms of total heat inflow q_i , total heat outflow q_o , and average Nusselt number (Nu_{avg}) when the transient simulation reaches a steady-state condition (and $q_i = q_o$). These quantities are calculated considering local Nusselt number (Nu) of heating walls of the protruded heater and cooling walls of the enclosure as detailed below.

Nu for left, right and top surfaces of a protruded heater (or of the enclosure) are given by,

$$Nu_l = -\frac{\partial\theta}{\partial X}\bigg|_{\text{left wall}}, Nu_r = -\frac{\partial\theta}{\partial X}\bigg|_{\text{right wall}}, \text{ and } Nu_t = -\frac{\partial\theta}{\partial Y}\bigg|_{\text{top wall}}, \text{ respectively.} \tag{5}$$

Using above relations, the heat inflow and average Nusselt number for the single heater and the two heaters are formulated using dimensionless height ($H = h/L$) and width ($W = w/L$) of heater and interspatial distance ($D = d/L$) as

$$q_{i,1H} = \int_0^H Nu_l dY + \int_{0.5(L-W)}^{0.5(L+W)} Nu_r dX + \int_0^H Nu_t dY \tag{6}$$

$$q_{i,2H} = \left(\int_0^H Nu_l dY + \int_{0.5(L-D)-W}^{0.5(L-D)} Nu_r dX + \int_0^H Nu_t dY \right) + \left(\int_0^H Nu_l dY + \int_{0.5(L+D)}^{0.5(L+D)+W} Nu_r dX + \int_0^H Nu_t dY \right) \tag{7}$$

$$Nu_{avg,1H} = \frac{q_{i,1H}}{2H + W} \text{ and } Nu_{avg,2H} = 0.5 \frac{q_{i,2H}}{2H + W} \tag{8}$$

whereas, the heat outflow from both the single heater and two-heater enclosures and Nu_{avg} on the basis of all the cold walls are expressed by

$$q_o = \int_0^1 Nu_l dY + \int_0^1 Nu_r dY \text{ for side-side cold (SSC) configuration} \tag{9}$$

$$q_o = \int_0^1 Nu_l dY + \int_0^1 Nu_r dX + \int_0^1 Nu_t dY \text{ for side-top-side cold (STSC) configuration} \tag{10}$$

$$Nu_{avg,1HE} = q_o/2 \text{ and } Nu_{avg,2HE} = q_o/3 \tag{11}$$

Using Eqs. (8) and (11), the overall heat transfer coefficients for all heating surfaces and enclosure’s cooling surfaces can be computed separately in an integrated manner. The prediction of heat transfer on the basis of total surface area will be more useful for the designing of such system, as it takes care of both symmetric and asymmetric flow structures that may occur in the cavity.

The steady-state heat transfer mechanism from the protruded heater to the enclosure’s walls is analyzed using heatlines [19–22] as it can describe heat transport properly while the convection mode is present. It takes into account of both the conductive and convective heat fluxes. Heatfunction equations for present study are expressed in the first-order differential form as

$$-\frac{\partial\Pi}{\partial X} = V\theta - \frac{\partial\theta}{\partial Y} \text{ and } \frac{\partial\Pi}{\partial Y} = U\theta - \frac{\partial\theta}{\partial X} \tag{12}$$

Heatlines (that indicate constant heatfunctions) are generated using the solved velocity and temperature fields as a part of post-processing, by solving Eq. (12) iteratively following an integration method. In similar way, streamfunction equations for the protruded heater enclosures are solved and utilized to represent overall fluid-flow pattern in the flow domain in terms of streamlines (constant streamfunctions), which are defined as

$$-\frac{\partial\psi}{\partial X} = V \text{ and } \frac{\partial\psi}{\partial Y} = U \tag{13}$$

The streamfunction on the outer surface of flow domain is set to zero as the boundary walls are impermeable, while a reference point with zero value is chosen at the middle of bottom wall of the enclosure for the solution of heatfunction equations.

Apart from flow visualization, the streamfunction, in this work, is used to extract global information regarding the total flow occurring in the cavity and the state of flow whether symmetric or asymmetric. Under natural convection, the maximum or minimum value of streamfunction indicates the amount of fluid-flow induced from differential heating of the enclosure. In a confined enclosure the induced flow appears in the form of recirculation or vortex, and it may be one or many, symmetric or asymmetric vortices depending upon the problem specification (distribution of thermal conditions on the cavity) and values of involved parameters (Ra , Pr). Under the circumstances a tool is necessary that can measure the overall quantity of induced flow irrespective of number of circulation vortices present in the cavity. To handle this situation in a general way, an approach of magnitude sum (without sign) of all ψ at the centre of individual vortices is conceived and the same is utilized in this work as an estimate for total fluid flow (ψ_{tot}), expressed as

$$\psi_{tot} = \sum_{k=1}^n |\psi_k| \quad (14)$$

where, n indicates number of recirculation vortices. It can be used for a single circulation situation where $\psi_{tot} = |\psi|_{\max}$ and for two symmetric or asymmetric circulations where $\psi_{tot} = \psi_{\max} + |\psi_{\min}|$. It should be mentioned here that for two or more circulations usually ψ_{\max} or ψ_{\min} is used, which could not be a good indicator to reflect the total flow occurring in a cavity as it indicates a part-flow occurring in some portion of entire flow domain. The proposed ψ_{tot} can address single- to multi-vortical flow situation and can provide a comparable basis.

3 Results and discussion

To attain the stated objectives of present work, the numerical simulations are carried out by placing a single heater as well as double heaters symmetrically on the

bottom wall of the enclosure under two different thermal boundary conditions (SSC and STSC) for a range of Rayleigh numbers (10^3 – 10^6) considering two commonly used working fluids, air ($Pr = 0.71$) and water ($Pr = 6.9$). For double heaters, the study is extended for three interspatial distances ($D = 0.1, 0.2$ and 0.3), as the distance influences the heat transfer process and flow structure. Only the steady-state results are presented in this work ignoring all the transient behaviors. As expected from the symmetric heating at bottom and cooling from sidewalls or side and top walls, in general, the hot fluid rises up along the mid-vertical plane of the enclosure and descends along cold sidewalls for all the cases considered in this work. It results the formation of two primary dominating circulations in the left and right halves of the enclosure. Heat flows from the protruded heater through the working fluid to the cold walls of the enclosure. However, the natures of heat and fluid flow depend on heater number (single or double) and height (or aspect ratio A), enclosure thermal condition (SSC or STSC), type of working fluid (air or water), driving strength of buoyancy force (expressed in terms of Ra) and interspatial distance (D) for double heaters.

The work is organized to emphasize fluid and energy flow structures in the cavity using streamlines and heatlines, first for single protruded heater enclosure and then for double protruded heater enclosure considering air and $Ra \leq 10^5$ with respect to different heater aspect ratios. The effect of interspatial distance on the flow structures is presented next for $Ra = 10^6$. Thereafter, the analyses of heat transfer and thermally-induced buoyancy flow for both the heater configurations are carried out in comprehensive manner for air. Afterwards, the study of water based single and double heater enclosures is discussed following the same structure as used for air.

3.1 Study of single heater enclosure using air ($Pr = 0.71$)

The heat transport from heater to fluid and from fluid to enclosure's walls is governed by thermally-induced convection in the enclosure. The area of fluid-domain decreases as the height of the protruded heater increases. The relative dominance of convection over conduction depends upon Rayleigh number (Ra), and

the convection is stronger at higher Ra. Accordingly, the numerical simulation of the single heater enclosure is conducted at different Ra by varying the heater height for both the thermal conditions (SSC, STSC) and the corresponding results of isotherms, streamlines and heatlines are presented with respect to heater aspect ratio (A) for a Ra value in top, middle and bottom panels, respectively, in Figs. 2 (for SSC) and 3 (for STSC) for $Ra = 10^3$ and 10^5 .

3.1.1 Effect of aspect ratio under SSC thermal condition

The effect of aspect ratio and Ra value on the energy and fluid flow structures under SSC thermal condition is presented in Fig. 2. The evolution of isotherm contours with the increase in heater aspect ratio can be realized along each row of respective Ra in Fig. 2. For each case, non-dimensional temperature is varying from 1 at heater surface to 0 at sidewalls of the enclosure. Accordingly, the isotherm contours are distributed surrounding the periphery of the heater towards the sidewalls in a particular manner. However, the width of the temperature bands (distance between any two consecutive isotherms of equal interval) evidently reduces with the increase in aspect ratio due to the increase in enthalpy input in the enclosure for the same Ra. At lower $Ra = 10^3$ due to weaker circulation velocity, heat transport from the heater surface is mainly governed by conduction mode. Most of the isotherms, in the form of layers of similar curves, enclose the heating body with the adiabatic bottom wall of the enclosure. In the second row of this figure, two counter-rotating circulations mirrored about the mid-vertical plane are formed for all values of A . The cores of circulations are slightly shifted upwards with the increase in heater height. Heatlines for $Ra = 10^3$ shown in the third row are generated from the surfaces of the heater and ended to either sidewalls symmetrically. The heat energy is directly transported through the well-bordered corridors of heatlines. The value of maximum heatfunction is evidently increases with the increase in heater aspect ratio as noticeable from heatline contour value near the bottom of the enclosure.

As Ra increases ($Ra = 10^5$), in the fourth row, the surrounded isotherms are densely distributed over the

heating surfaces indicating a sharp temperature variation therein and the rest of the isotherms are connected between the adiabatic bottom and top walls orthogonally. The fluid-flow pattern inside the enclosure changes with aspect ratio due to increase in heater height, however the fluid rotates symmetrically in anti-clockwise (at left) and clockwise (at right) directions as the heater are located at the middle of bottom wall. The fluid nearby heater being hot moves upward like a plume along the mid-vertical plane of the enclosure and is deflected at top adiabatic wall towards either sidewalls. Afterwards, it descends down in releasing heat along the cold vertical walls. The values of ψ at the centre of left circulation vortex for different aspect ratio are sequentially mentioned in the caption of Fig. 2. This indicates that the strength of the circulation increases as A increases up to certain value ($A = 1$) due to higher heat input, thereafter decreases due to reduction in fluid volume in the enclosure.

Heatlines for $Ra = 10^5$ (last row of Fig. 2) are also symmetric and markedly concentrated along mid-vertical plane, indicating a flow of intense energy flux. At $Ra = 10^5$ the strength of convective heat flux increases and forms energy recirculation indicated by closed-loop heatlines. The rate of heat transfer is much higher compared to that of $Ra = 10^3$ due to strong convection and again increases with A .

3.1.2 Effect of aspect ratio under STSC thermal condition

The flow features of single protruded heater enclosure under STSC are shown in Fig. 3. In this case, the top wall of the enclosure is allowed to exchange heat along with sidewalls, and the heat transfer characteristics become different compared to that of earlier SSC configuration.

Marked changes compared to isotherm patterns of earlier SSC case are observed in this case. All the isotherms surround the heater, originate from bottom wall and end thereon like inverted U, irrespective of Ra and A values. However, overall circulation patterns, compared to SSC configuration, remain almost unchanged with STSC configuration; two symmetrical fluid circulations are observed in the cavity. Significant changes are observed in heatlines distribution. In the third row for $Ra = 10^3$, heatlines from the

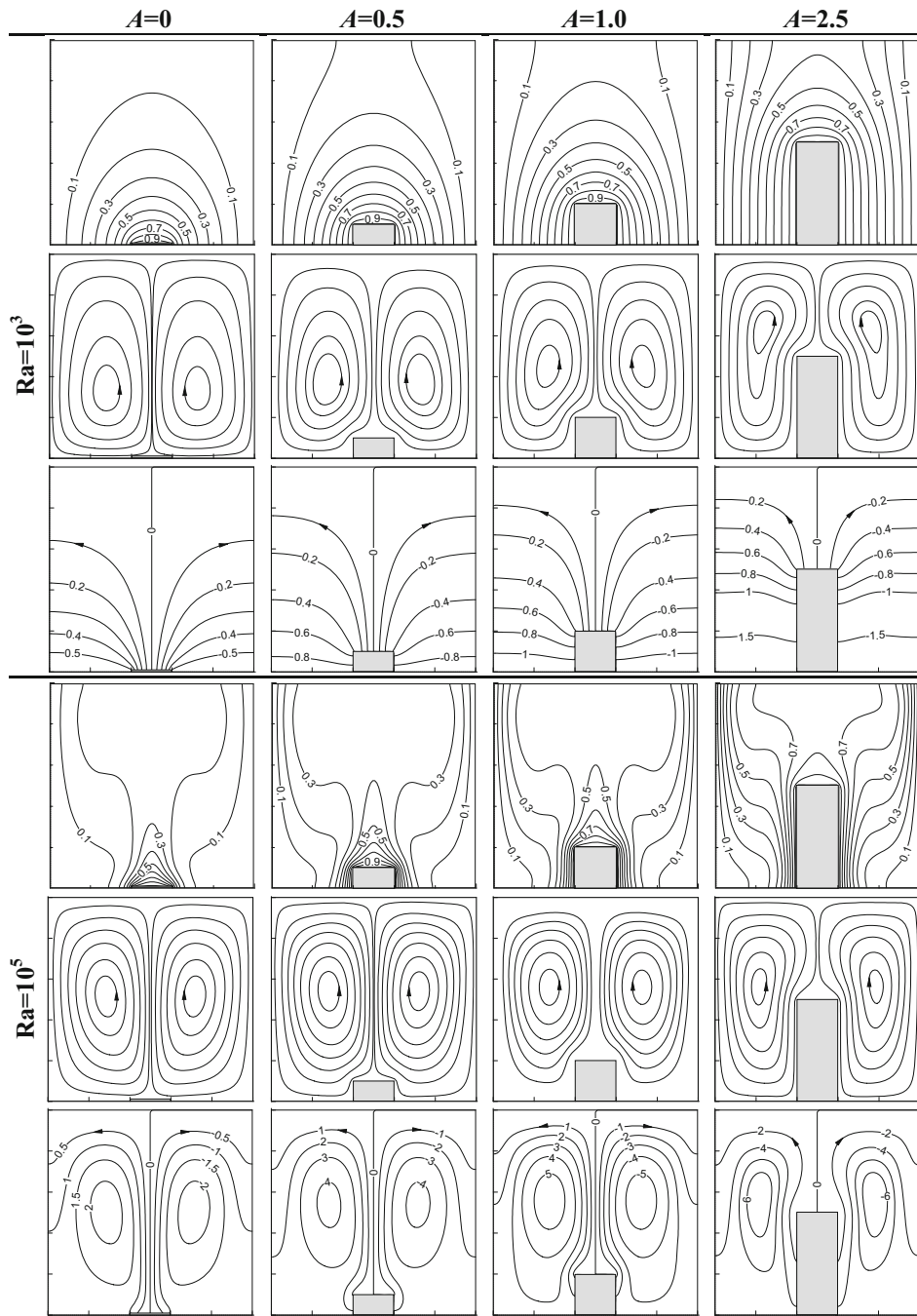


Fig. 2 Visualization of flow fields of single heater enclosure using air under SSC configuration at different A (0–2.5), Ra (10^3 , 10^5): isotherms (top panel), streamlines (middle panel) and heatlines (bottom panel) for each case of Ra . For $A = 0$ –2.5, $\psi = 0.151, 0.205, 0.217, 0.185$ at $Ra = 10^3$, and $\psi = 9.840, 11.940, 12.158, 9.649$ at $Ra = 10^5$

protruded heater are distributed over the three walls (at top, left and right) in a straightforward manner due to conduction dominant flow. However, when Ra is

moderately high, at $Ra = 10^5$ heatlines form closed-loop circulations due to high convective heat flux. The rate of heat transfer increases. For both Ra values as A

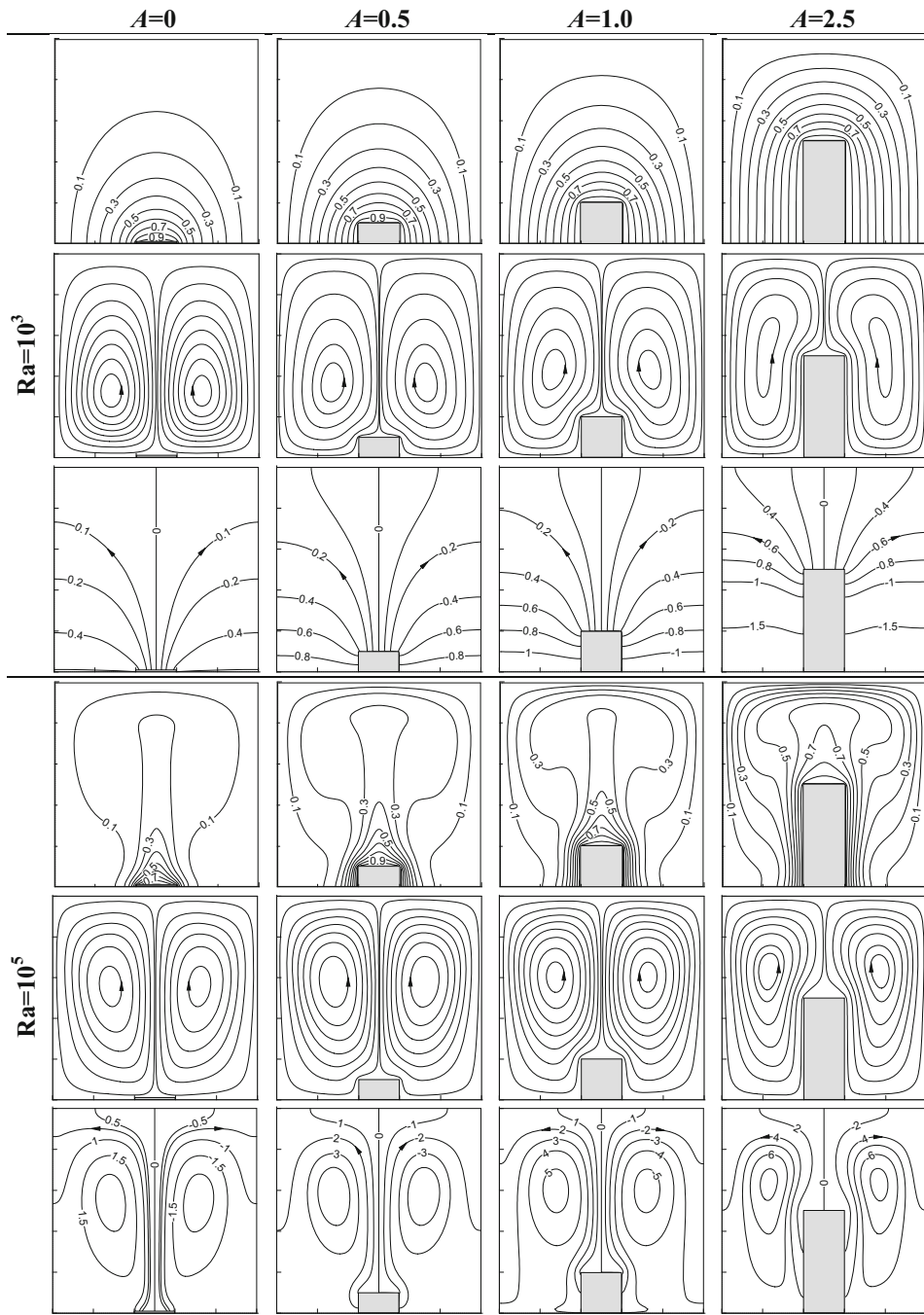


Fig. 3 Visualization of flow fields of single heater enclosure using air under STSC configuration at different A (0–2.5), Ra (10^3 , 10^5): isotherms (top panel), streamlines (middle panel) and heatlines (bottom panel) for each case of Ra . For $A = 0–2.5$, $\psi = 0.146, 0.196, 0.203, 0.162$ at $Ra = 10^3$, and $\psi = 10.630, 13.252, 13.984, 11.659$ at $Ra = 10^5$

increases, more amount of heat from the top surface of the protruded heater is directly absorbed by the top cold wall of the enclosure. Flow patterns are

symmetric, and ψ at the centre of left circulation vortex changes with A as mentioned in the caption of Fig. 3.

3.2 Study of double heater enclosure using air ($Pr = 0.71$)

The results of double heater enclosure for the SSC and STSC conditions at different Ra , A , and interspatial distance (D) are presented systematically in Figs. 4, 5, 6 and 7.

3.2.1 Effect of aspect ratio under SSC condition

Figure 4 shows the evolution of mass and energy transport structures in the presence of two identical protruded heaters under SSC configuration. The heaters are placed symmetrically about the mid-vertical plane of the enclosure at an interspatial distance of $D = 0.2$. With the double heaters, the isotherm contours also surround both the heaters as reflected from the plots for $Ra = 10^3$ and 10^5 along the first and fourth rows of Fig. 4.

At $Ra = 10^3$ isotherms make semicircular loops with bottom wall when $A < 1$, whereas most of the isotherms get connected between the adiabatic bottom and top walls at higher A . As Ra increases the hot fluids coming over two individual heaters are joined together and move upward along the mid-vertical plane like a hot plume, which is clearly indicated by the peaks of isotherm curves along the vertical mid-section.

In regard to streamline plots, two symmetric circulations are located over the heater. For flushed-heaters ($A = 0$), the streamline patterns are almost identical for both the cases of single heater (Fig. 3) and double heaters (Fig. 4). For other A , the size of the primary circulations drastically reduces with the increase in aspect ratio. The size of fluid-circulations particularly at higher $A = 2.5$ markedly shrinks as the fluid volume and obstruction-free space inside the enclosure are reduced significantly.

At $Ra = 10^3$, end-to-end heatlines are observed between the heaters and the sidewalls of the enclosure, which provide direct transfer of energy from the heater to the cold sidewalls through the slowly rotating pool of fluid. Over the each sidewall heat is transferred non-uniformly with a higher rate at the bottom. This trend becomes reversed at higher $Ra = 10^5$ due to the formation of energy recirculation cells indicated by closed-loop heatlines. Heatlines near the top wall are parallel as this wall is adiabatic. It is interesting to note that the heatlines originating from the outer sides of

two heater travel longer path to reach their nearest walls when $A \leq 1$. However, when $A = 2.5$, from lower part of these outer surfaces, the heat flows to the nearest sidewalls following the shortest route. Recirculation-free heat transportation is observed at lower Ra for all A . In contrast, energy circulation persists for all A at higher $Ra = 10^5$, with decreasing in size. The energy recirculation cells are significantly lifted up at higher $A = 2.5$. Two minor circulations of mass and energy fill up the space in-between two heaters for all protruded heaters irrespective of A . As mentioned in caption of Fig. 4, ψ value is found to decrease from $A = 1$, due to the reduction in more fluid volume in the presence of two heaters.

3.2.2 Effect of aspect ratio under STSC configuration

The effects of aspect ratio and Ra value on the flow fields under STSC thermal condition of double heater enclosure are shown in Fig. 5. Three adjacent walls at left, top and right of the enclosure are cold. It results the isotherm distribution like inverted U as found in case of the single heater, but with a wide base due to the presence of two heaters. The either ends of isotherm contours are located on the same bottom wall of the enclosure. At $Ra = 10^3$ as heat transfer is dominated by conduction mode and isotherms are distributed in regular manner without any distortions. The distortions appear at higher $Ra = 10^5$ due to stronger recirculation velocities at the outer region of circulation vortices. This stronger velocity deflects isotherms towards sidewalls at top, whereas at lower portion, pushes them towards the heaters' top.

The mass transport patterns are similar for both Ra values, however the vortex strength is higher with increased Ra due to stronger convection. The aspect ratio also affects similar way, with reducing vortex size at higher A . At $Ra = 10^3$ end-to-end heatlines from one heater are distributed over one sidewall and half of top wall of the respective side. The energy recirculation cells are formed at $Ra = 10^5$. The heat transfer is found to increase with increasing A due to convection dominant flow.

3.2.3 Effect of interspatial distance between two heaters at $Ra = 10^6$

The effect of interspatial distance (D) between two protruded heaters on the flow structures is shown in

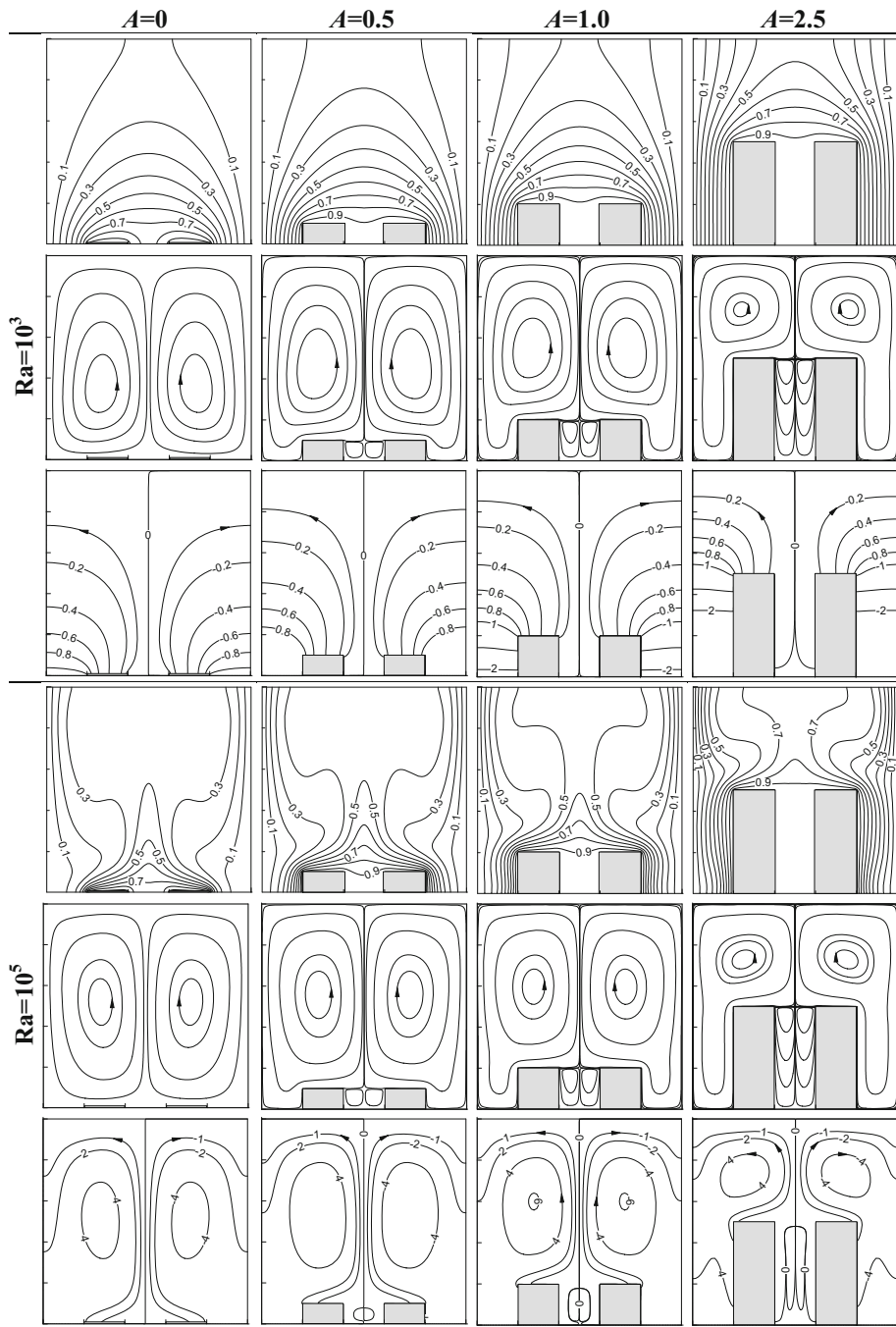


Fig. 4 Visualization of flow fields of double heater enclosure using air under SSC configuration at different A (0–2.5), Ra (10^3 , 10^5): isotherms (top panel), streamlines (middle panel) and heatlines (bottom panel) for each case of Ra . For $A = 0–2.5$, $\psi = 0.176, 0.192, 0.187, 0.119$ at $Ra = 10^3$, and $\psi = 12.792, 12.942, 12.130, 7.365$ at $Ra = 10^5$

Fig. 6 for both SSC and STSC conditions at $Ra = 10^6$ and $D = 0.1$ and 0.3 using three aspect ratios, $A = 0, 1$ and 2.5 .

A close inspection of isotherms and heatlines in Fig. 6 reveals that the heat transfer increases marginally with higher $D = 0.3$ for all A values of SSC

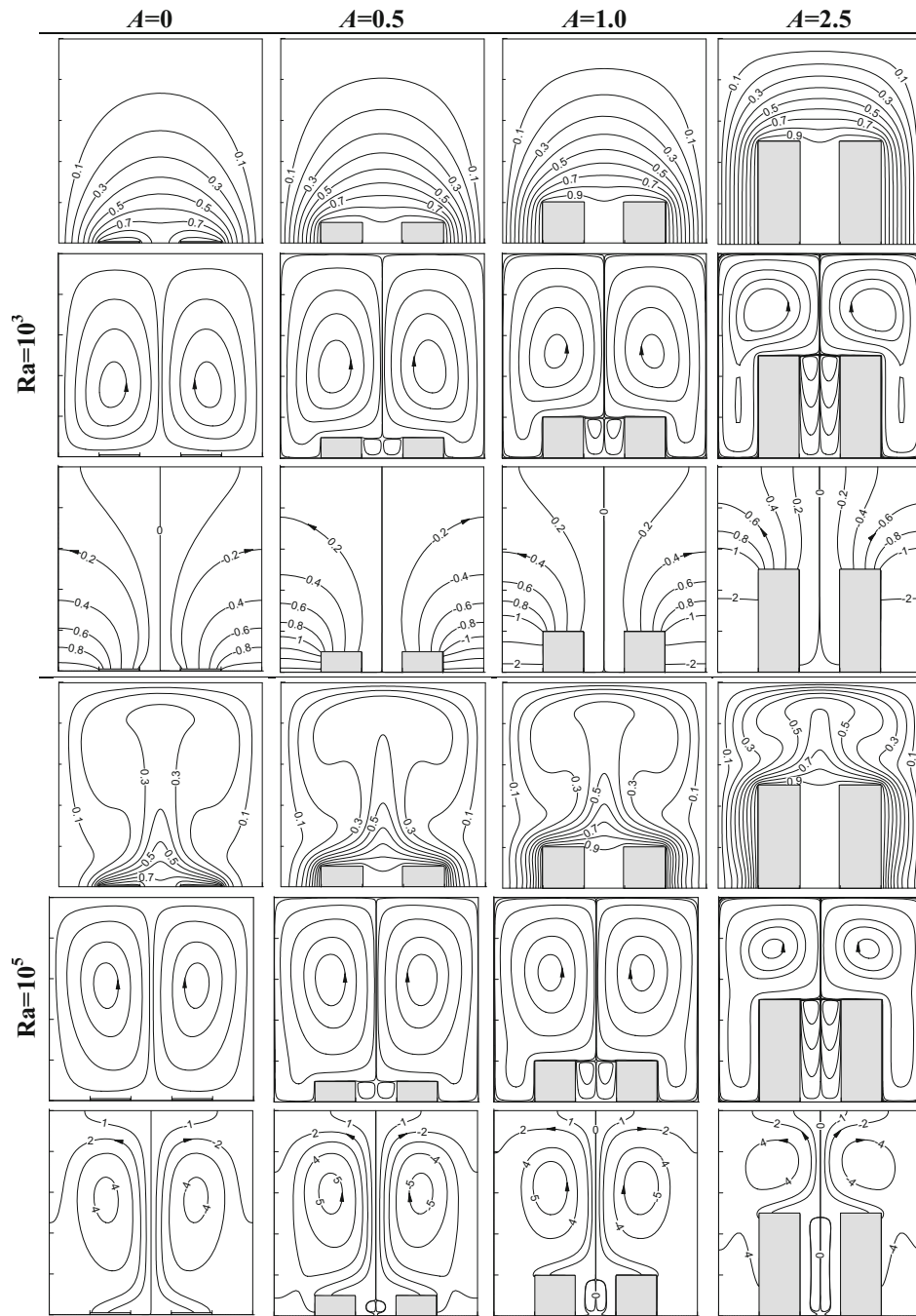


Fig. 5 Visualization of flow fields of double heater enclosure using air under STSC configuration at different A (0–2.5), Ra (10^3 , 10^5): isotherms (top panel), streamlines (middle panel) and heatlines (bottom panel) for each case of Ra . For $A = 0$ –2.5, $\psi = 0.168$, 0.176, 0.162, 0.083 at $Ra = 10^3$, and $\psi = 13.963$, 14.438, 13.868, 9.500 at $Ra = 10^5$

condition (Fig. 6a) and for STSC (Fig. 7b) up to $A = 1$. ψ values as noted in figure caption indicate the same fact of higher circulation strength with the higher

value of D . The size of minor vortices in between the two heaters increase with increased D . Under STSC with smaller $D = 0.1$ at $A = 2.5$ (Fig. 6b and column

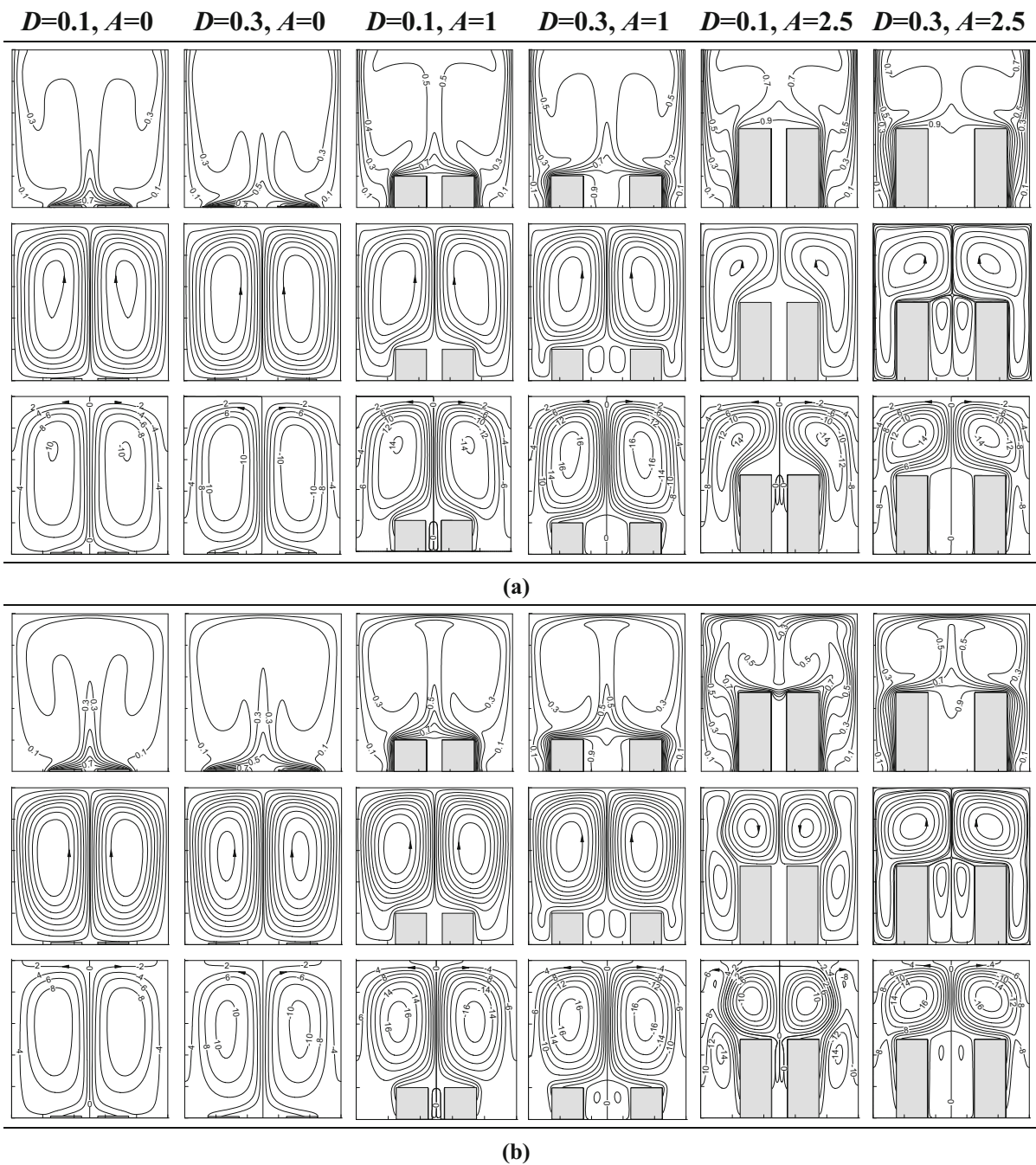


Fig. 6 Effect of interspatial distance on isotherms (*top panel*), streamlines (*middle panel*) and heatlines (*bottom panel*) at $Ra = 10^6$ for air: **a** SSC, **b** STSC. For $A = 0-2.5$, $\psi = 31.683$,

33.974, 28.682, 31.924, 20.434, 20.978 for SSC, and $\psi = 41.364, 41.752, 44.910, 44.163, (26.448, 17.563), 32.364$ for STSC

5), some interesting flow structures are observed. An inverted plume replaces the rising-plume like isotherm contour that consistently appeared along mid-vertical

plane as if originating from the cold top wall. In addition to this, horn-shaped isotherms appear at the outer top corners of two protruded heaters. Why it

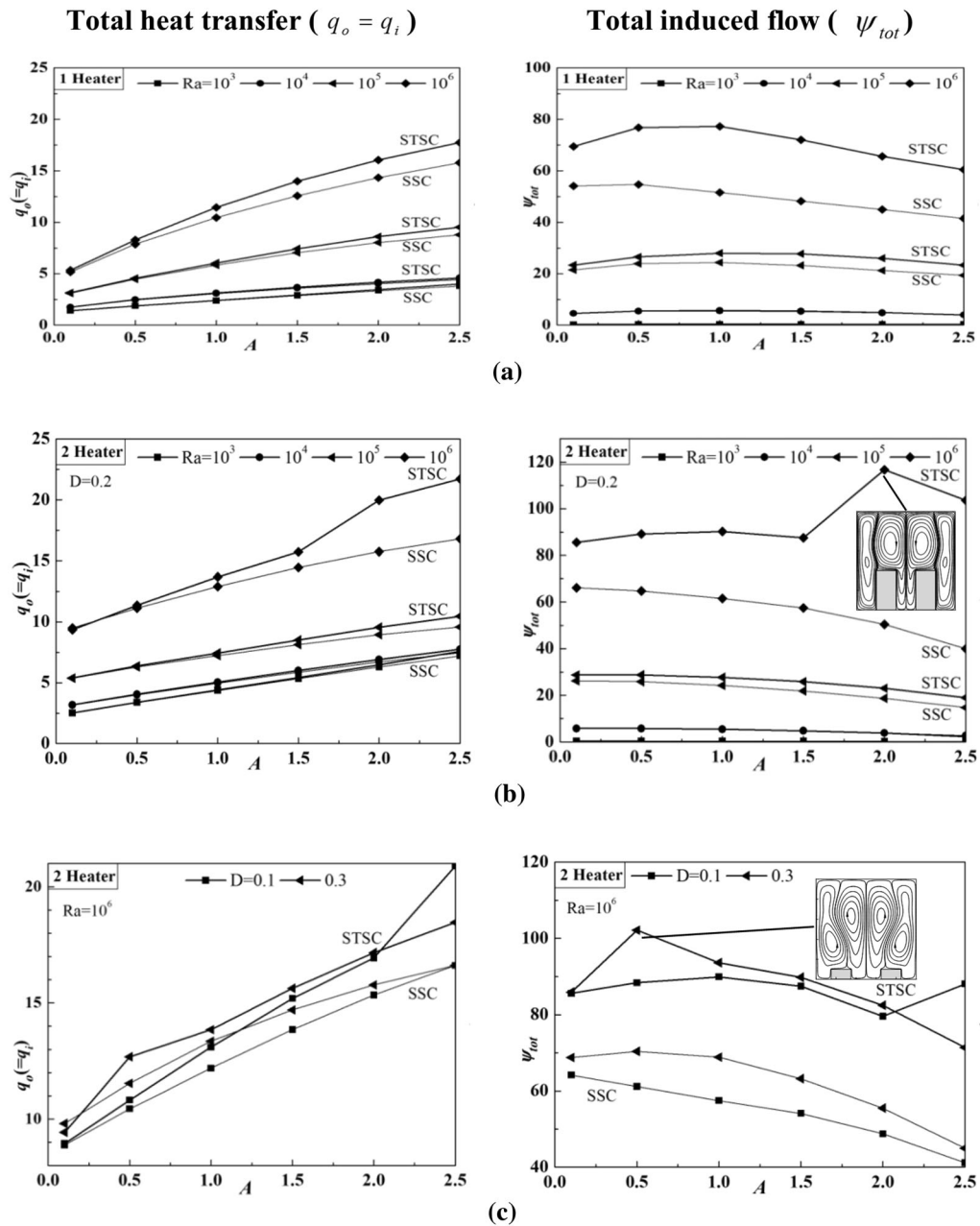


Fig. 7 Assessment of total heat transfer (q_o or q_i) and total induced flow (ψ_{tot}) under SSC and STSC using air for **a** single heater enclosure, **b** double heater enclosure and **c** interspatial heater distance

happens so can be understood by observing the streamlines patterns. Here, the earlier-seen two primary circulations are broken down into four significant vortices. The newly formed vortices over the heater top rotate in opposite direction to their mother circulations. The breaking of primary circulation (which are sufficiently stronger $\psi = 26.448, 17.563$, and involve with higher velocity) is happened due to the failure of taking sharp-turn over the heater towards the mid-vertical axis within a short distance ($D = 0.1$). In case of $D = 0.3$, it gets sufficient space to execute gradual turning as could be seen from corresponding streamline plot. This peculiarity (as seen for isotherms and streamlines) is carried forward for the transport of heat in the form of four energy recirculation cells. Two significant energy circulations for each half of the flow-domain are observed in heatline plot, and heat transfer is found to increase significantly. All flow-fields structures shown in Fig. 6 indicate that the flow structure of air at $Ra = 10^6$ is symmetric irrespective of D (as well as thermal condition).

3.3 Trends of global parameters for air

The trends of heat transfer and induced flow in the presence of the protruded heater are presented in Fig. 7 in terms of q_o ($=q_i$ at steady state) and ψ_{tot} . As explained in Sect. 2 in connection with Eq. (14), that ψ_{tot} is a magnitude sum (without sign) of minimum and maximum streamfunctions of all vortices and measures the total thermally-induced flow occurring in the enclosure irrespective of number of recirculation vortices and their symmetric or asymmetric appearance. It could be a powerful analyzing tool to handle complex flow structures consisting of multiple significant circulations as found in this work for double heaters under STSC shown in column 5 of Fig. 6b and as shown in Fig. 7b, c. The results reveal that both the heat transfer (q_o) and total flow (ψ_{tot}), in comparison with SSC condition, significantly increases under STSC condition when $Ra \geq 10^5$ for both single and double protruded heaters (Fig. 7a, b), due to greater cooling surface under STSC condition. Heat transfer (q_o) increases with the heater aspect ratio for both single (Fig. 7a) and double (Fig. 7b) heater enclosures, as heating surface area increases with the increase in the heater aspect ratio. In contrast, the total

induced flow (ψ_{tot}) steadily decreases as the aspect ratio increases particularly after $A > 1$, due to the reduction in fluid volume in the cavity for single heater enclosure, irrespective of Ra value. As higher rate of heating occurs in the presence of double protruded heaters, so with it q_o and ψ_{tot} are found comparatively higher than that of single protruded heater. At higher Ra (10^6), sudden difference in trends of q_o and ψ_{tot} are observed under STSC condition when A increases above 1.5. ψ_{tot} increases significantly due to breaking of two primary vortices into the four as shown in inset of Fig. 7b, and corresponding heat transfer also increases (Fig. 7b). The interspatial distance between the two protruded heaters (Fig. 7c) also cause some marked influences on the natural convection in the enclosure, and the trend depends on heater aspect ratio particularly for STSC condition. In general the heat transfer increases at $D = 0.2$, that is, when the heaters are located from the wall at a distance same as the interspatial distance. Heat transfer increases remarkably at $A \geq 2$ under STSC condition. Compared to SSC, STSC yields high fluid flow ψ_{tot} as found for q_o , due to greater heat transfer (through the increased cooling surface at top) causing higher circulation velocity. Moreover, ψ_{tot} is found higher at lower A ($=0.5$) due to vortex break-up (shown in inset of Fig. 7c).

3.4 Study of protruded heater enclosure using water ($Pr = 6.9$)

The study of the protruded heater is extended to investigate the submerged passive cooling using water ($Pr = 6.9$) as working fluid for both SSC and STSC conditions in the range of $Ra = 10^3$ – 10^6 . The results show that up to $Ra = 10^5$ fluid and energy flow structures, and isotherm distribution are similar to that of air, pattern-wise. The symmetric flow fields, as found for air, are observed for all A values when $Ra \leq 10^5$ irrespective of number of heater and imposed thermal boundary condition considered in this work. So the corresponding flow structures are not presented here, for brevity. The flow structures of water corresponding to $Ra = 10^6$, when the convection plays significant dominant role on the flow, is considered for illustration in the form of comparison with those of air in following subsections.

3.4.1 Single protruded heater enclosure

The simulated results of single heater enclosure at $Ra = 10^6$ for both water ($Pr = 6.9$) and air ($Pr = 0.71$) are presented for SSC and STSC conditions in Figs. 8 and 9, respectively. The flow structures are found to be symmetric for both water (Figs. 8a, 9a) and air (Figs. 8b, 9b) under both the thermal conditions. The basic trends of all these flow fields resemble to the trends that observed for air at $Ra = 10^5$. In Fig. 8 during the convection dominant flow at $Ra = 10^6$, the isotherms for both water and air are densely localized at the heater surfaces and the enclosure surfaces, and their distortions are more pronounced here. Comparing the isotherms of water with that of air, particularly with contour values of 0.2 at $A = 0$ and 0.3 at $A = 0.5$, it seen that area of hotter fluid region is higher for high Prandtl-fluid water. A thin thermal boundary is formed near the enclosure's walls and it becomes thinner with the increase in heater aspect ratio for the same Ra , due to the reduction in the velocity boundary layer thickness. The streamline patterns are symmetric about mid-vertical plane for all the cases of aspect ratios and fluids shown in Fig. 8, however the position and shape of their circulation cores differ. With air the core is significantly lifted upward, whereas the same of water at different aspect ratio is found to be located about a half-height distance of the distance between the heater top and the top of enclosure wall. The value of ψ_{\max} (or ψ_{\min}) is comparatively higher for water due to higher heat transfer through greater thermal conductivity. The end-to-end heatlines between the heater surfaces and the enclosure sidewalls and the closed-loop recirculating heatlines are observed in all the cases. The maximum heatfunctions of water is higher than those of air, indicating higher rate of heat transfer is possible using water.

In Fig. 9, the changes with respect to same-valued contours of water and air are well marked. For both the fluids, the cooling at top cold wall (since STSC) is significant, as indicated by concentrated isotherms thereon. Heatlines originating from the heater are distributed over the three enclosure walls, and also form energy recirculation. The lifting of vortex cores as found for SSC condition of air is not prominent under STSC

condition due to availability of top cooling. The observations regarding the effect of aspect ratio remain almost unchanged. However, under STSC condition the heat transfer with water is marginally increased compared to that of air.

3.4.2 Double protruded heater enclosure

The results corresponding to the double heater enclosure are shown in similar way as above in Figs. 10 and 11 for water and air at $Ra = 10^6$. The isotherms, streamlines and heatlines of water ($Pr = 6.9$) in Fig. 10a at $A = 0.5, 1$, and Fig. 11a at $A \leq 1$ show an asymmetric distribution. However, for the same in case of air in Figs. 10b and 11b, the flow symmetry is found to exist about mid-vertical plane with $Ra = 10^6$ irrespective of the imposed thermal boundary condition (SSC or STSC). In general the heat transfer is found intensified in the presence of two protruded heaters located at a distance of $D = 0.2$, indicated by concentrated contour lines in all the plots of isotherm. Comparing Fig. 10a with Fig. 11a, the flow asymmetry is strongly marked under STSC condition. It should be mentioned here that all the numerical simulations were carried out using transient forms of governing equations as mentioned in Eqs. (1)–(4) and no-oscillating behaviors were noted at the steady-state solutions. Apart from flow asymmetry, the breaking of primary circulations is observed in the last column of Fig. 11 for both the fluids under STSC condition. The four significant recirculation cells are formed as noted and discussed earlier in case of air with interspatial heater distance $D = 0.1$ in column 5 of Fig. 6b. Perhaps through this breaking of circulation the flow is maintained symmetry for water at higher aspect ratio $A = 2.5$.

3.4.3 Effect of interspatial distance with water ($Pr = 6.9$)

The influence of interspatial distance between two heaters on the asymmetric flow structures (as noted earlier in Figs. 10, 11) of water is shown in Fig. 12 for both SSC and STSC conditions. Under SSC, the fluid and energy flow structures and isotherms are perfectly

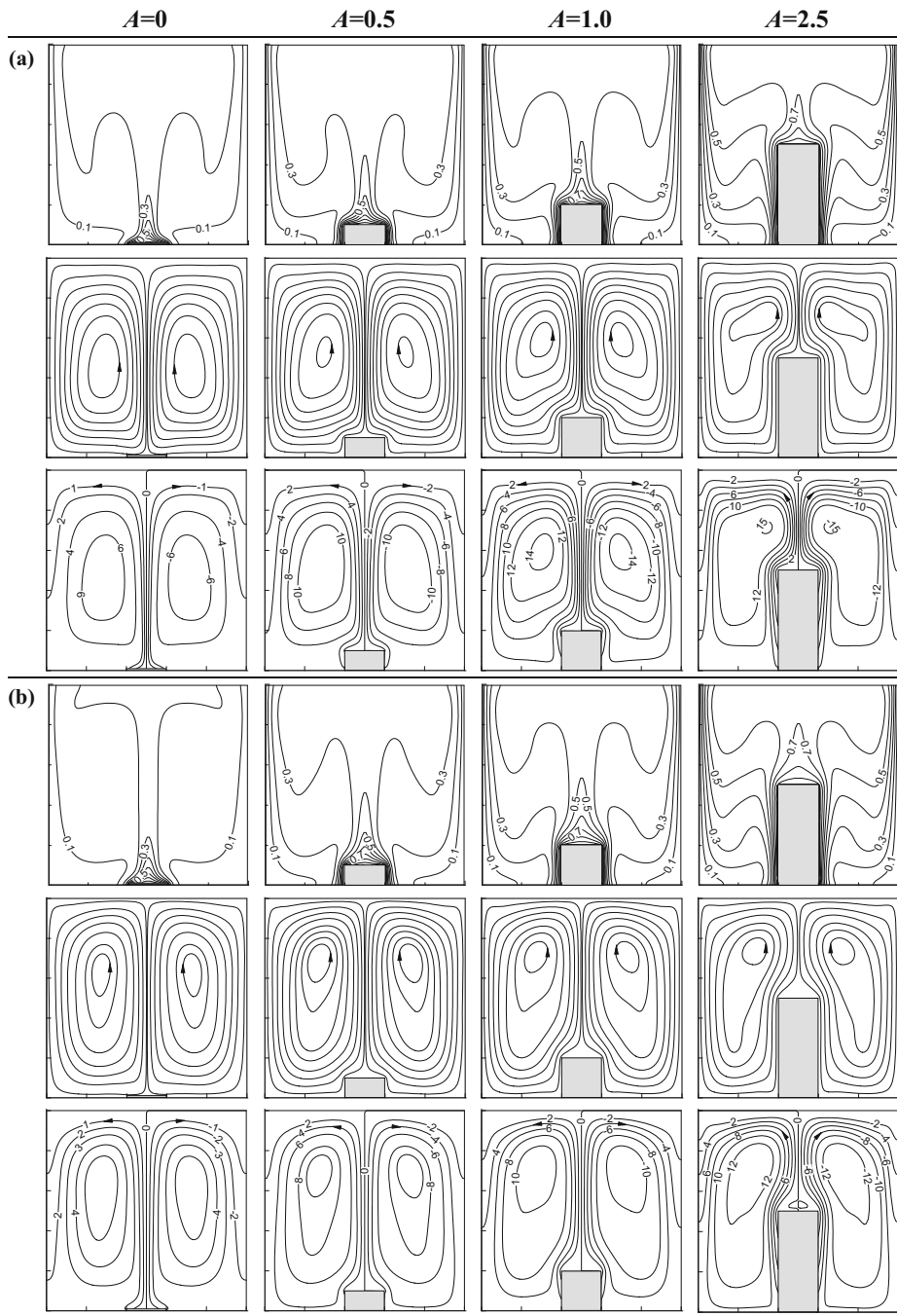


Fig. 8 Visualization of isotherms (*top panel*), streamlines (*middle panel*) and heatlines (*bottom panel*) of single heater enclosure under SSC condition at different A (0–2.5) for $Ra = 10^6$: **a** water ($Pr = 6.9$), $\psi = 32.845, 35.646, 34.238, 23.838$, **b** air ($Pr = 0.71$), $\psi = 26.066, 27.357, 25.782, 20.736$

symmetry irrespective of the heater aspect ratio when interspatial heater distance is small ($D = 0.1$), as indicated in Fig. 12a. But the symmetry breaks at the

higher distance ($D = 0.3$), which is clearly observed when $A \geq 1$. The same is not applicable to STSC shown in Fig. 12b. With the flushed-heater ($A = 0$),

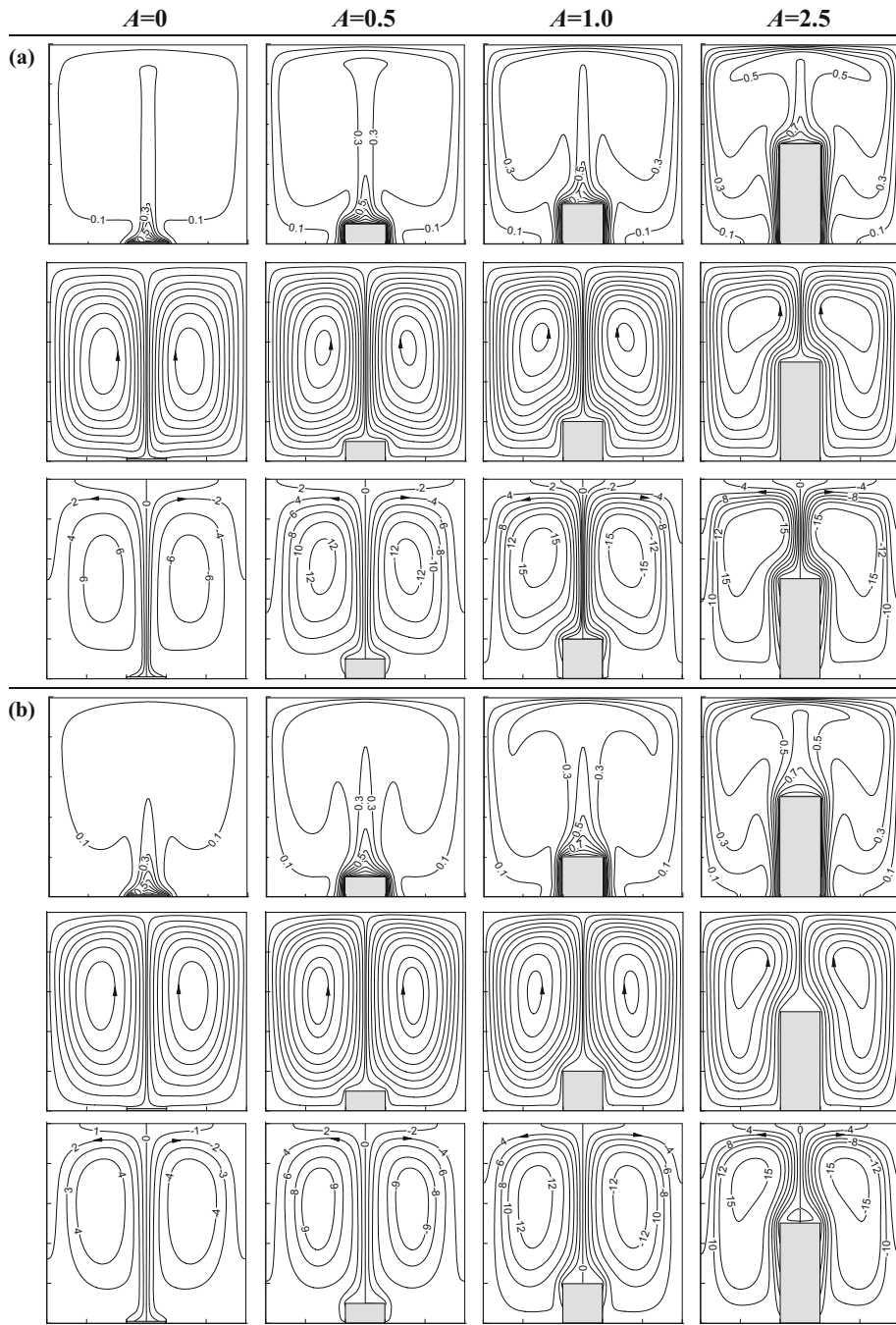


Fig. 9 Visualization of isotherms (*top panel*), streamlines (*middle panel*) and heatlines (*bottom panel*) of single heater enclosure under STSC at different A (0–2.5) for $Ra = 10^6$: **a** water ($Pr = 6.9$), $\psi = 38.307, 45.142, 46.096, 34.395$, **b** air ($Pr = 0.71$), $\psi = 32.680, 38.365, 38.368, 30.267$

the asymmetry persists irrespective of values of D . The higher value of D consistently generates asymmetric flow-fields patterns irrespective of A . When the

distance is closer ($D = 0.1$), the flow symmetry is governed by the two primary fluid and energy circulations at $A = 1$ and $A = 2.5$.

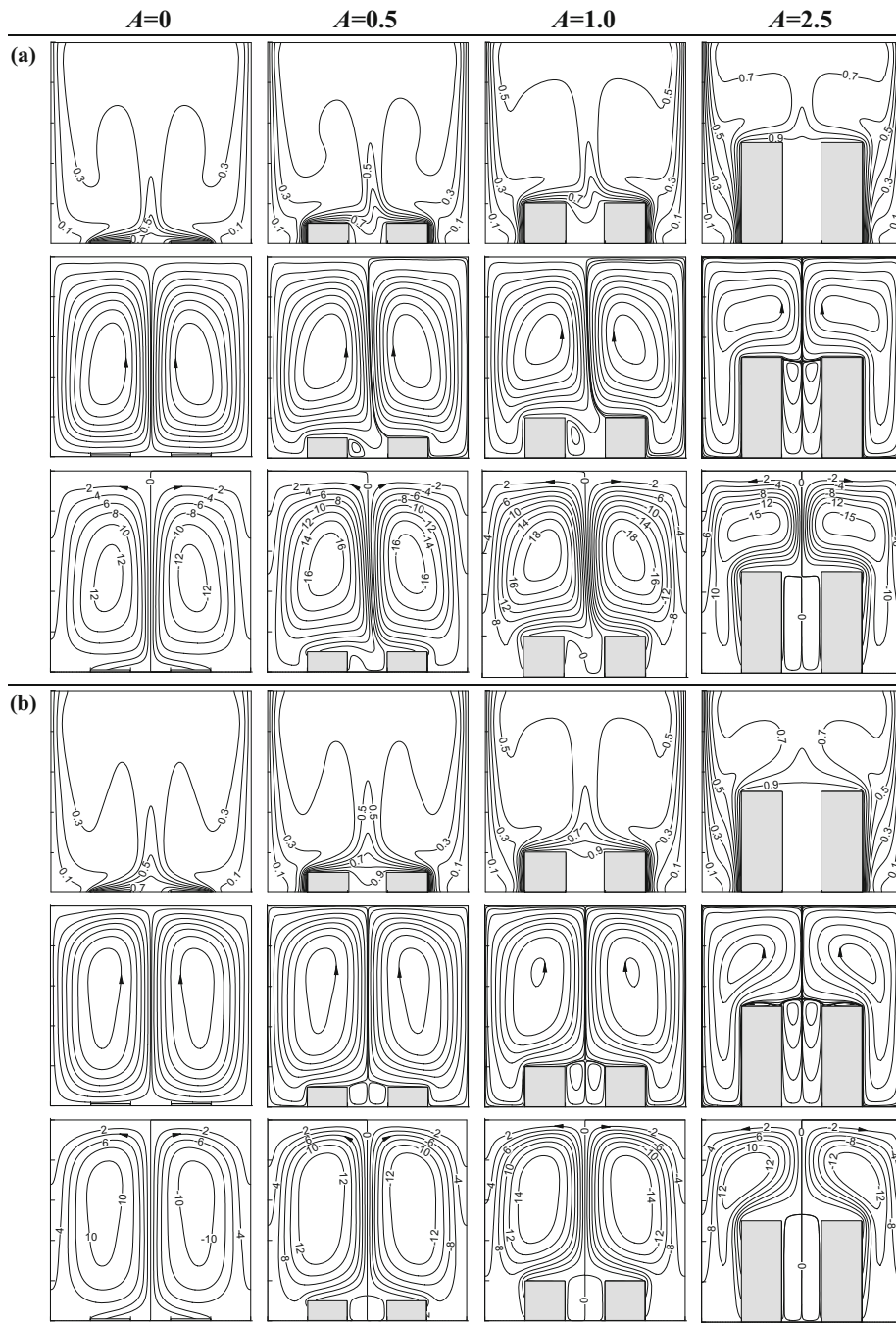


Fig. 10 Visualization of isotherms (top panel), streamlines (middle panel) and heatlines (bottom panel) of double heater enclosure under SSC condition at different A (0–2.5) for $Ra = 10^6$: **a** water ($Pr = 6.9$), $\psi = 39.637, 40.422, 38.175, 22.559$, **b** air ($Pr = 0.71$), $\psi = 32.616, 31.892, 30.342, 19.863$

The sharing of heat transfer among the cold walls is greatly influenced by the asymmetric recirculation, as can be understood from heatline

plots under STSC condition in Fig. 12b. At $A = 0$, the heat transfers through the left and the right sidewalls are not alike. The position, size and

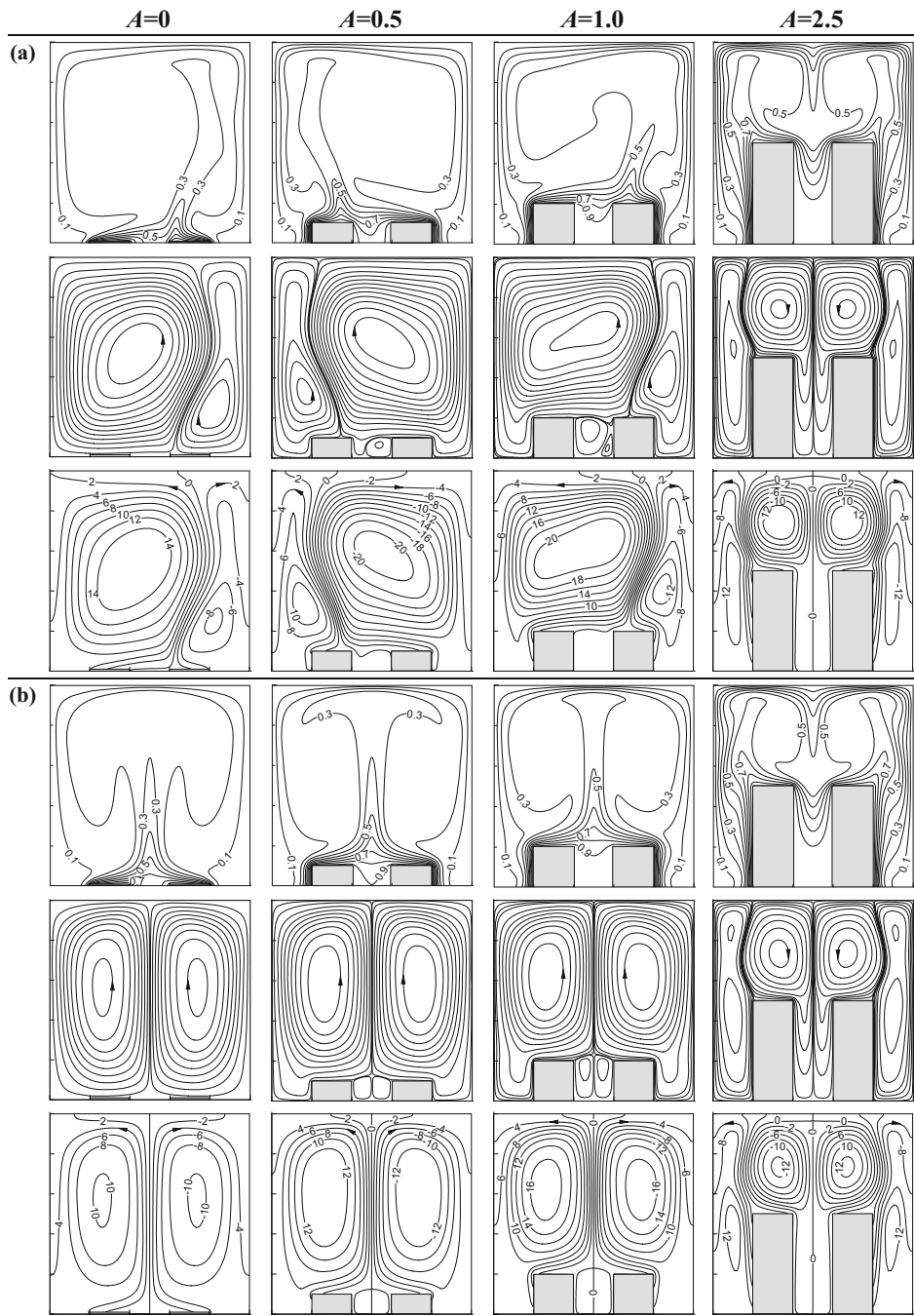


Fig. 11 Visualization of isotherms (*top panel*), streamlines (*middle panel*) and heatlines (*bottom panel*) of double heater enclosure under STSC at different A (0–2.5) for $Ra = 10^6$: **a** water ($Pr = 6.9$), $\psi = 59.844, 26.951, 52.768, 31.498$, **b** air ($Pr = 0.71$), $\psi = 41.419, 44.054, 44.594, 26.886$

orientation of core zones of mass and energy recirculation are not consistent with the varying degree of associated asymmetry. The degree of

asymmetry, and type and number of solutions are analyzed further using the tool of symmetric indicators later in Sect. 3.6.

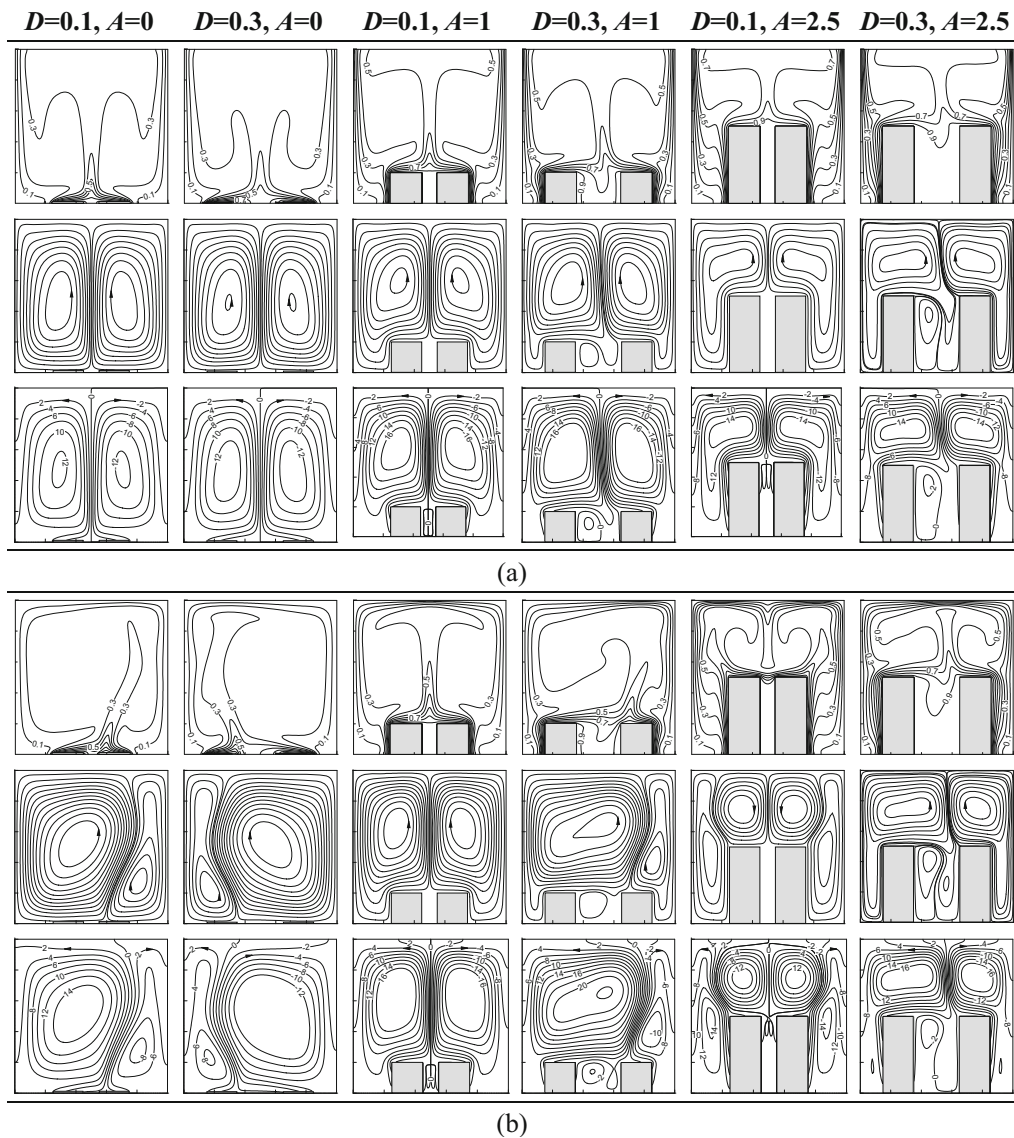


Fig. 12 Effect of interspatial distance on isotherms (*top panel*), streamlines (*middle panel*) and heatlines (*bottom panel*) at $Ra = 10^6$ for water: **a** SSC condition, **b** STSC condition. For

$A = 0-2.5$, $\psi = 38.896, 40.219, 36.30, 39.10, 22.516, 22.437$ for SSC, and $\psi = 59.715, 24.101, 49.629, 52.379, (30.811, 18.834), 32.364$ for STSC

3.5 Trends of global parameters for water (Pr = 6.9)

The trends of heat transfer and induced flow in the presence of the protruded heater using water are presented in Fig. 13 in terms of q_o and ψ_{tot} . ψ_{tot} can take care of the cases of symmetric, asymmetric, and

multi-vortex flow situations as observed with $Pr = 6.9$. The results show a monotonous rise of heat transfer (q_o) with the increase in heater aspect ratio for single protruded heater in Fig. 13a, and also for two protruded heaters in Fig. 13b. Up to $A = 1$ and $Ra < 10^5$, no significant change is noted in q_o between SSC and STSC conditions. The closer interspatial

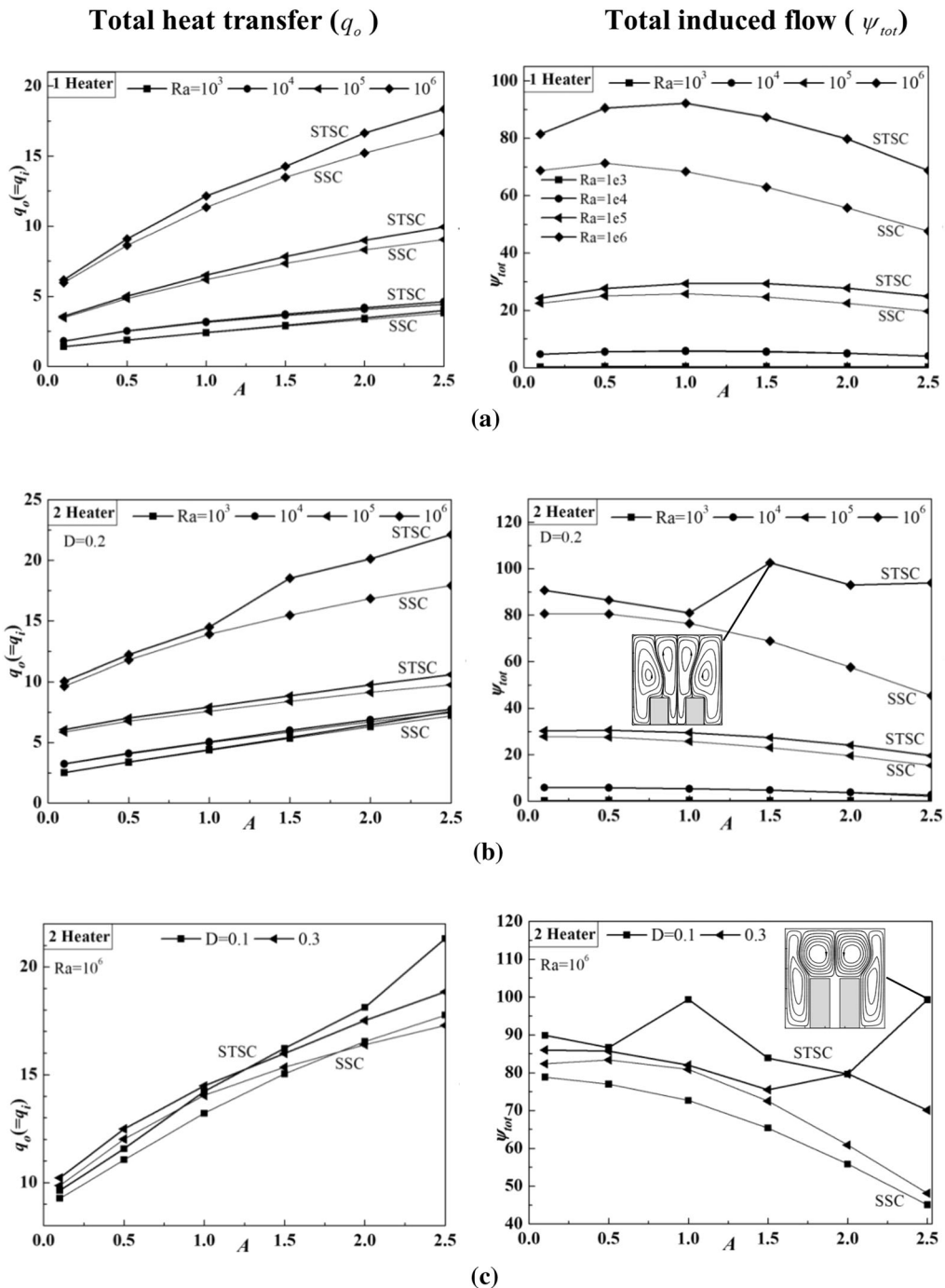


Fig. 13 Assessment of total heat transfer ($q_o = q_i$) and total induced flow (ψ_{tot}) under SSC and STSC configurations using water for **a** single heater enclosure, **b** double heater enclosure and **c** interspatial heater distance

distance (Fig. 13c) cause lesser heat transfer, in general. Heat transfer is remarkably high for $D = 0.2$ under STSC, as also found earlier for the case of air.

In regard to total flow (ψ_{tot}), the monotonous trends are maintained throughout except for STSC at $Ra = 10^6$. With the aspect ratio ψ_{tot} , though tries to increase somewhat due to increased circulation from

higher heat input through larger heater surface area, falls consistently with the increase in aspect ratio due to reduction in fluid volume and flow space. In case of STSC condition of double heaters ψ_{tot} appears in zigzag manner (as seen from Fig. 13b, c) due to strong asymmetric feature in the flow structure. ψ_{tot} is consistently found higher with STSC compared to SSC, as the heat transfer with STSC condition is relatively higher. The formations of multiple significant vortices are shown in Fig. 13b, c.

3.6 Bifurcation analysis

Although the heating and cooling are done symmetrically about the mid-vertical plane, the asymmetry in flow-field structures is found to evolve as seen in Fig. 11a for $Pr = 6.9$ with two protruded heaters. It inspires to conduct further study to explore the nature of asymmetry evolved in the cavity. The detailed analysis of vortical flow feature is performed by choosing the heater aspect ratio (A) and distance between two heaters (D) as 1.0 and 0.2, respectively. Simulations are executed by gradual increasing Ra from 10^3 to 10^6 (forward study) and gradual decreasing Ra from 10^6 to 10^3 (backward study) for both SSC and STSC thermal conditions. The results are post-processed using usual temperature based symmetry indicator (I_θ) as mentioned in [31] and a novel streamfunction based symmetry indicator (I_ψ), respectively expressed by

$$I_\theta = \int_0^1 \int_0^1 (\theta(X, Y) - \theta(1.0 - X, Y))^2 dX dY \quad (15)$$

$$I_\psi = \left(\sum_{k=1}^n \psi_k / \sum_{k=1}^n |\psi_k| \right)^2 \quad (16)$$

where, X and Y indicate the position of temperature nodes, dX and dY are the width and height of the individual (computational) cell. It is to be noted that the computational grids are mirrored about the mid-vertical plane of the enclosure. I_ψ is formulated in normalized form by considering the sense of rotation of each individual vortices through a sum along with the sign of ψ , and utilizing ψ_{tot} mentioned earlier in Eq. (14).

The analyses of the flow-field structures for the present problem are demonstrated in Fig. 14 using two

symmetric indicators (I_θ and I_ψ) expressed by Eqs. (15) and (16). Results in Fig. 14 shows both I_ψ and I_θ satisfy zero value for air ($Pr = 0.71$), indicating a perfectly symmetry flow structure about the mid-vertical plane for entire studied range of Ra , irrespective of heater numbers (one heater, two heaters) and thermal conditions (SSC, STSC). The symmetry is also found to maintain for water ($Pr = 6.9$) with single protruded heater irrespective of thermal boundary conditions and Ra values.

However for water ($Pr = 6.9$) with double heaters after a critical Ra , the departure from symmetry ($I \neq 0$) or a symmetry breaking bifurcation is observed in Fig. 14 under both the SSC and STSC conditions. In case of SSC condition, the critical point is noted at $Ra = 4 \times 10^5$, and the forward and back travel of solutions have traced the same path indicating a supercritical bifurcation. Development of gradual asymmetry is indicated through snapshots of isotherm (in I_θ plot of Fig. 14a) and streamline (in I_ψ plot of Fig. 14b) for SSC configuration. For STSC configuration, subcritical bifurcation with a clear hysteresis phenomenon is observed for Ra in between 1.5×10^5 and 6×10^5 . Subcritical bifurcation was also observed by Ridouane and Campo [32] in a bottom-heated isosceles triangle. In case of forward simulation as Ra increases above the critical value of 2×10^5 , I increases monotonically up to $Ra = 6 \times 10^5$ and the central main plume shifts towards left (Coanda effect) causing asymmetric circulations in the cavity as indicated by corresponding flow-field snapshots shown on the figures (Fig. 14c, d). However after $Ra = 6 \times 10^5$ with further increase in Ra , no significant change occurs in the overall flow structure, which is indicated by a small change in I value due to some minor adjustments in flow fields. In case of the backward simulation with decreasing Ra from the highest value of 10^6 , the strength of the convective flow gets reduced progressively; and the steady-state solutions take place following a separate path below $Ra = 6 \times 10^5$ till $Ra = 1.5 \times 10^5$. With the decreasing Ra the left circulation vortex augments in size and pushes the main plume towards mid-vertical plane.

For both types of bifurcation, the developed I_ψ shown in Fig. 14b, d indicates the same values of all critical Ra indicated by I_θ (shown in Fig. 14a, c). However, as expected (from different quantities and

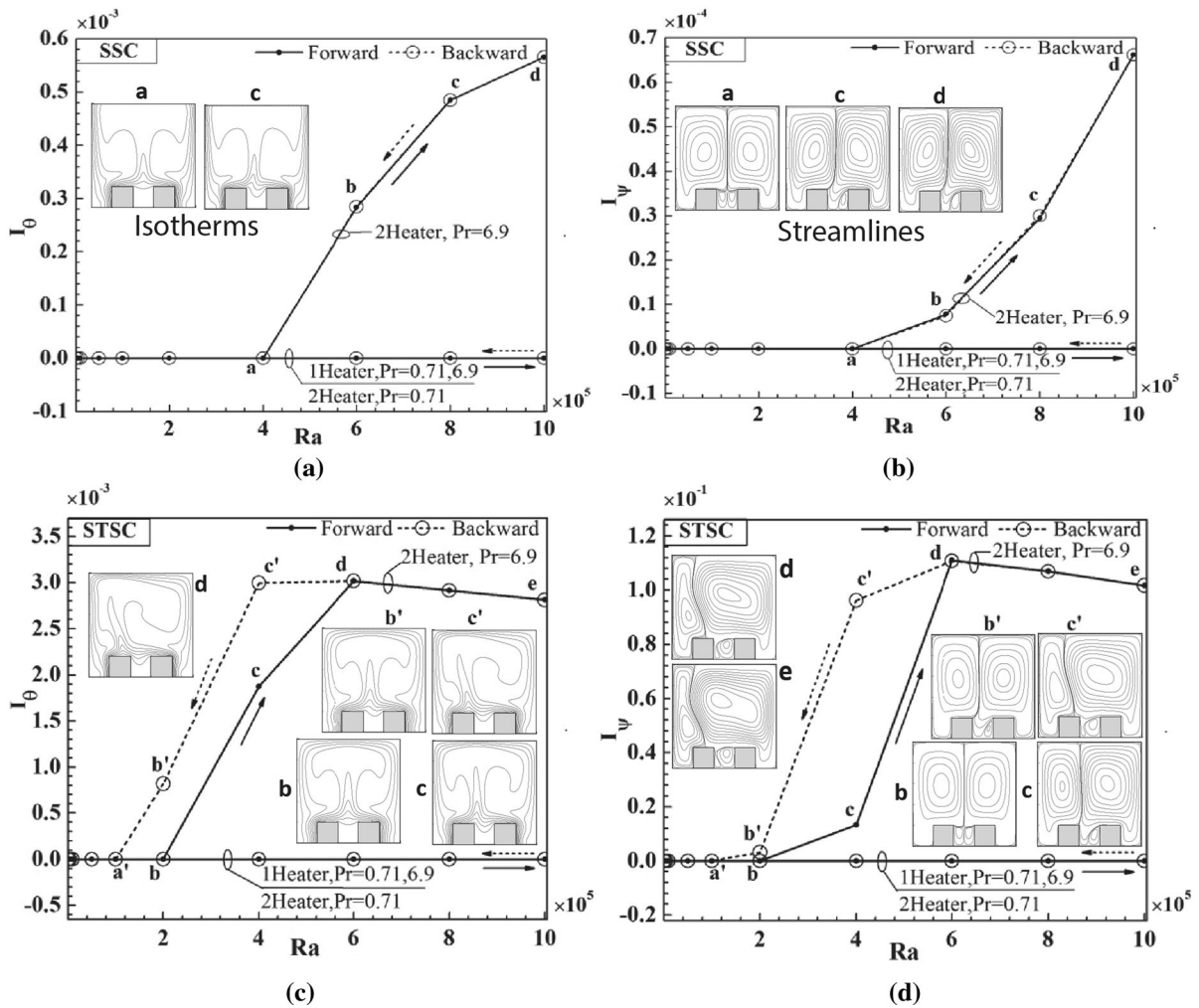


Fig. 14 Symmetry analysis of flow-field structures of protruded heater enclosures considering single and double heaters (at aspect ratio $A = 1$), and SSC and STSC thermal conditions

formulae) the orders of magnitudes of I_ψ and I_θ are different. The comparison of I_ψ and I_θ in Fig. 14 suggests that the developed I_ψ can be utilized as a new tool for symmetry or bifurcation analysis.

4 Conclusions

The present work investigates buoyancy-driven flow using a single and double protruded heaters of various aspect ratios in a square enclosure using air ($Pr = 0.71$) and water ($Pr = 6.9$) under two different thermal boundary conditions, one with side-side cooled (SSC) configuration and other with side-top-

both for air ($Pr = 0.71$) and water ($Pr = 6.9$); temperature based symmetry analysis (shown in a, c at the left) and vortical structure based symmetry analysis (shown in b, d at the right)

side cooled (STSC) configuration, for Rayleigh number (Ra) ranging from 10^3 to 10^6 . The energy flow along with usual fluid flow is investigated using Bejan’s heatlines and streamlines considering bottom-mounted, protruded heaters positioned symmetrically about mid-vertical plane of the enclosure. The salient observations of this work are as follows:

- The energy flow from the protruded heater to the cold walls of the enclosure is taken place through a set of well-defined corridors formed by the end-to-end heatlines between the heater surfaces and the enclosure walls without energy recirculation cells when $Ra \leq 10^4$ and with energy recirculation when $Ra \geq 10^5$.

- Heat transfer with STSC thermal boundary condition is consistently found to be higher compared to that with SSC condition. Heat transfer using water is superior to that using air. Heat transfer using double heaters becomes higher.
- Increasing heater aspect ratio increases heat transfer, but decreases the induced fluid flow due to reduction in fluid volume.
- The flow structures for the case of air are symmetric within the study range ($Ra \leq 10^6$) for both the single and double heaters irrespective of the thermal condition and interspatial heater distance.
- Breaking of primary circulations and formation of peculiar flow structures are observed with the changes of boundary condition, heater height and fluid.
- The flow structures for the case of water are found to be symmetric for single heater for all Ra values, and also for double heaters when $Ra \leq 10^5$. After $Ra = 10^5$ a significant asymmetric flow structures are observed, which strongly depends on heater height (or aspect ratio), interspatial distance, and applied thermal condition. SSC thermal condition and smaller interspatial distance favor more towards the formation of symmetric flow structure.
- A novel concept of summation of maximal and minimal streamfunctions of individual vortices is developed and utilized to estimate the total induced flow in the enclosure.
- With the heater height, a consistent trend of increasing heat transfer with decreasing total flow is noted in the study.
- The evolved flow asymmetry is also addressed through a bifurcation analysis using both temperature based symmetry indicator I_θ , and streamfunction based symmetry indicator I_ψ . Both the symmetry indicators coherently measure the degree of asymmetry of the obtained solutions. I_ψ is a major outcome of this work and could be utilized as an investigating tool for the analysis of the state of flow.
- Within the study range of Ra (10^3 – 10^6), the symmetry solutions are observed for air ($Pr = 0.71$) irrespective of number of heaters or thermal conditions.
- However for water ($Pr = 6.9$), the symmetry persists with the single protruded heater for all

ranges of Ra. It persists also with double protruded heaters up to $Ra = 10^5$, afterwards the flow becomes asymmetric. The nature of asymmetric solutions strongly depends on imposed thermal condition on the enclosure. Under SSC thermal condition, supercritical bifurcation is observed after a critical $Ra = 4 \times 10^5$; whereas, subcritical bifurcation is found under STSC condition after a critical $Ra = 1.5 \times 10^5$.

Present work reveals an important fact on asymmetric flow feature for double protruded heaters with water as working fluid ($Pr = 6.9$) under symmetrical heating and cooling configuration. Interestingly we have observed both supercritical and subcritical bifurcation depending upon the thermal boundary condition of the enclosure.

Acknowledgments The present authors would like to thank anonymous reviewers for their comments and valuable suggestions, which have improved the quality of this manuscript. The authors also wish to acknowledge helpful discussions with Prof. Dipankar Sanyal and Prof. Achintya Mukhopadhyay, Department of Mechanical Engineering, Jadavpur University.

References

1. Ostrach O (1988) Natural convection in enclosures. *J Heat Transf* 110:1175–1190
2. Incropera FP (1988) Convection heat transfer in electronic equipment cooling. *J Heat Transf* 110:1097–1111
3. GdeV Davies (1983) Natural convection of air in a square cavity: a bench-mark numerical solution. *Int J Numer Methods Fluids* 3:249–264
4. Narasimham GSVL (2010) Natural convection from discrete heat sources in enclosures: an overview. *Vivechan Int J Res* 1:63–78
5. Mukhopadhyay A (2010) Analysis of entropy generation due to natural convection in square enclosures with multiple discrete heat sources. *Int Commun Heat Mass Transf* 37:867–872
6. Banerjee S, Mukhopadhyay A, Sen S, Ganguly R (2008) Natural convection in a bi-heater configuration of passive electronic cooling. *Int J Therm Sci* 47(11):516–527
7. Aydin O, Yang WJ (2000) Natural convection in enclosures with localized heating from below and symmetrical cooling from sides. *Int J Numer Methods Fluids* 10(5):519–529
8. Sharif MAR, Mohammad TR (2005) Natural convection in cavities with constant flux heating at the bottom wall and isothermal cooling from the sidewalls. *Int J Therm Sci* 44:865–878
9. Calcagni B, Marsili F, Paroncini M (2005) Natural convective heat transfer in square enclosures heated from below. *Appl Therm Eng* 25:22–31

10. Varol Y, Oztop HF, Yilmaz T (2007) Natural convection in triangular enclosures with protruding isothermal heater. *Int J Heat Mass Transf* 50:2451–2462
11. Paroncini M, Corvaro F (2009) Natural convection in a square enclosure with a hot source. *Int J Therm Sci* 48:1683–1695
12. Corvaro F, Paroncini M (2009) An experimental study of natural convection in a differentially heated cavity through a 2D-PIV system. *Int J Heat Mass Transf* 52:355–365
13. Corvaro F, Paroncini M (2009) The natural convective heat transfer in a partially divided enclosure: a study on the influence of the source position. *J Thermodyn* 2009:1–10
14. Nardini G, Paroncini M, Corvaro F (2014) Effect of heat transfer on natural convection in a square cavity with two source pairs. *Heat Transf Eng* 35(9):875–886
15. AlAmiri A, Khanafer K, Pop I (2009) Buoyancy-induced flow and heat transfer in a partially divided square enclosure. *Int J Heat Mass Transf* 52:3818–3828
16. Bakkas M, Hasnaoui M, Amahmid A (2010) Natural convective flows in a horizontal channel provided with heating isothermal blocks: effect of the inter blocks spacing. *Energy Convers Manag* 51:296–304
17. Baik C-I, Lee K-S, Kim W-S (1997) Study of combined heat transfer in a three dimensional enclosure with a protruding heat source. *Numer Heat Transf A* 32:733–747
18. Dagtekin I, Oztop HF (2001) Natural convection heat transfer by heated partitions within enclosure. *Int Commun Heat Mass Transf* 28(6):823–834
19. Kimura S, Bejan A (1983) The heatline visualization of convective heat transfer. *J Heat Transf ASME* 105(4):916–919
20. Costa VAF (2006) Bejan's heatlines and masslines for convection visualization analysis. *Appl Mech Rev* 59:126–145
21. Basak T, Roy S (2008) Role of Bejan's heatlines in heat flow visualization and optimal thermal mixing for differentially heated square enclosures. *Int J Heat Mass Trans* 51:3486–3503
22. Dalal A, Das MK (2008) Heatline method for the visualization of natural convection in a complicated cavity. *Int J Heat Mass Transf* 51:263–272
23. Biswas N, Mahapatra PS, Manna NK, Roy PC (2015) Influence of heater aspect ratio on natural convection in a rectangular enclosure. *Heat Transf Eng* 37(2):1–15
24. Alfieri F, Tiwari M, Zinovik KI, Brunschweiler T, Michel B, Poulidakos D (2012) On the significance of developing boundary layers in integrated water cooled 3D chip, stacks. *Int J Heat Mass Transf* 55:5222–5232
25. Kota K, Hidalgo P, Joshi Y, Glezer A (2009) Thermal management of a 3D chip stack using a liquid interface to a synthetic jet cooled spreader. In: 15th International workshop thermal investigations ICs and systems, Leuven, Belgium, pp 1–6
26. Kota K, Hidalgo P, Joshi Y, Glezer A (2010) A novel conduction-convection based cooling solution for 3d stacked electronics. In: 26th Annual IEEE semiconductor thermal measurement model management symposium, Santa Clara, CA, pp 1–8
27. Kota K, Hidalgo P, Joshi Y, Glezer A (2012) Hybrid liquid immersion and synthetic jet heat sink for cooling 3-D stacked electronics components. *IEEE Transf Packag Manuf Technol* 2(5):817–824
28. Bejan A (2004) *Convection heat transfer*, 3rd edn. Wiley, New York
29. Mahapatra PS, De S, Ghosh K, Manna NK, Mukhopadhyay A (2013) Heat transfer enhancement and entropy generation in a square enclosure in the presence of adiabatic and isothermal blocks. *Numer Heat Transf A* 64:576–597
30. Patankar SV (1980) *Numerical heat transfer and fluid flow*. Taylor and Francis, London
31. Bouafia M, Daube O (2007) Natural convection for large temperature gradients around a square solid body within a rectangular cavity. *Int J Heat Mass Transf* 50:3599–3615
32. Ridouane EH, Campo A (2006) Formation of a pitchfork bifurcation in thermal convection flow inside an isosceles triangular cavity. *Phys Fluids* 18:074102-1-8